Physics potential of a long-baseline neutrino oscillation experiment using a J-PARC neutrino beam and Hyper-Kamiokande

Hyper-Kamiokande Proto-Collaboration

K. Abe[57,59], H. Aihara[60,59], C. Andreopoulos[29], I. Anghel[23], A. Ariga[1], T. Ariga[1], R. Asfandiyarov[15], M. Askins[4], J. J. Back[65], P. Ballett[11], M. Barbi[43], G. J. Barker[65], G. Barr[41], F. Bay[14], P. Beltrame[13], V. Berardi[18], M. Bergevin[4], S. Berkman[3], T. Berry[47], S. Bhadra[70], F. d. M. Blaszczyk[31], A. Blondel[15], S. Bolognesi[7], S. B. Boyd[65], A. Bravar[15], C. Bronner[59], F. S. Cafagna[18], G. Carminati[5], S. L. Cartwright[49], M. G. Catanesi[18], K. Choi[35], J. H. Choi[9], G. Collazuol[20], G. Cowan[13], L. Cremonesi[46], G. Davies[23], G. De Rosa[19], C. Densham[53], J. Detwiler[66], D. Dewhurst[41], F. Di Lodovico[46], S. Di Luise[14], O. Drapier[12], S. Emery[7], A. Ereditato[1], P. Fernández[32], T. Feusels[3], A. Finch[28], M. Fitton[53], M. Friend[24,†], Y. Fujii[24,†], Y. Fukuda[34], D. Fukuda[39], V. Galymov[7], K. Ganezer[6], M. Gonin[12], P. Gumplinger[62], D. R. Hadley[65], L. Haegel[15], A. Haesler[15], Y. Haga[57], B. Hartfiel[6], M. Hartz[59,62], Y. Hayato[57,59], M. Hierholzer[1], J. Hill[6], A. Himmel[10], S. Hirota[26], S. Horiuchi[68], K. Huang[26], A. K. Ichikawa[26], T. Iijima[35,36], M. Ikeda[57], J. Imber[52], K. Inoue[55,59], J. Insler[31], R. A. Intonti[18], T. Irvine[58], T. Ishida[24,†], H. Ishino[39], M. Ishitsuka[61], Y. Itow[37,36], A. Izmaylov[22], B. Jamieson[67], H. I. Jang[51], M. Jiang[26], K. K. Joo[8], C. K. Jung[52,59], A. Kaboth[17], T. Kajita[58,59], J. Kameda[57,59], Y. Karadzhov[15], T. Katori[46], E. Kearns[2,59], M. Khabibullin[22], A. Khotjantsev[22], J. Y. Kim[8], S. B. Kim[50], Y. Kishimoto[57,59], T. Kobayashi[24,†], M. Koga[55,59], A. Konaka[62], L. L. Kormos[28], A. Korzenev[15], Y. Koshio[39,59], W. R. Kropp[5], Y. Kudenko[22,‡], T. Kutter[31], M. Kuze[61], L. Labarga[32], J. Lagoda[38], M. Laveder[20], M. Lawe[49], J. G. Learned[16], I. T. Lim[8], T. Lindner[62], A. Longhin[27], L. Ludovici[21], W. Ma[17], L. Magaletti[18], K. Mahn[33], M. Malek[17], C. Mariani[68], L. Marti[59], J. F. Martin[63], C. Martin[15], P. P. J. Martins[46], E. Mazzucato[7], N. McCauley[29], K. S. McFarland[45], C. McGrew[52], M. Mezzetto[20], H. Minakata[48], A. Minamino[26], S. Mine[5], O. Mineev[22], M. Miura[57,59], J. Monroe[47], T. Mori[39], S. Moriyama[57,59], T. Mueller[12], F. Muheim[13], M. Nakahata[57,59], K. Nakamura[59,24,†], T. Nakaya[26,59], S. Nakayama[57,59], M. Needham[13], T. Nicholls[53], M. Nirkko[1], Y. Nishimura[58], E. Noah[15], J. Nowak[28], H. Nunokawa[44], H. M. O'Keeffe[28], Y. Okajima[61], K. Okumura[58,59], S. M. Oser[3], E. O'Sullivan[10], T. Ovsiannikova[22], R. A. Owen[46], Y. Oyama[24,†], J. Pérez[32], M. Y. Pac[9], V. Palladino[19], J. L. Palomino[52], V. Paolone[42], D. Payne[29], O. Perevozchikov[31], J. D. Perkin[49], C. Pistillo[1], S. Playfer[13], M. Posiadala-Zezula[64], J.-M. Poutissou[62], B. Quilain[12], M. Quinto[18], E. Radicioni[18], P. N. Ratoff[28], M. Ravonel[15], M. A. Rayner[15], A. Redij[1], F. Retiere[62], C. Riccio[19], E. Richard[58], E. Rondio[38], H. J. Rose[29], M. Ross-Lonergan[11], C. Rott[54], S. D. Rountree[68], A. Rubbia[14], R. Sacco[46], M. Sakuda[39], M. C. Sanchez[23], E. Scantamburlo[15], K. Scholberg[10,59], M. Scott[62], Y. Seiya[40], T. Sekiguchi[24,†], H. Sekiya[57,59], A. Shaikhiev[22], I. Shimizu[55], M. Shiozawa[57,59], S. Short[46],

†Also at: J-PARC, Tokai, Japan.

‡Also at: Moscow Institute of Physics and Technology and National Research Nuclear University "MEPhI", Moscow, Russia.

§Also at: Institute of Particle Physics, Canada.

¶Also at: BMCC/CUNY, Science Department, New York, NY, USA.

G. Sinnis[30], M. B. Smy[5,59], J. Sobczyk[69], H. W. Sobel[5,59], T. Stewart[53], J. L. Stone[2,59],
Y. Suda[60], Y. Suzuki[59], A. T. Suzuki[25], R. Svoboda[4], R. Tacik[43], A. Takeda[57], A. Taketa[56],
Y. Takeuchi[25,59], H. A. Tanaka[3,§], H. K. M. Tanaka[56], H. Tanaka[57,59], R. Terri[46],
L. F. Thompson[49], M. Thorpe[53], S. Tobayama[3], N. Tolich[66],
T. Tomura[57,59], C. Touramanis[29], T. Tsukamoto[24,†], M. Tzanov[31], Y. Uchida[17],
M. R. Vagins[59,5], G. Vasseur[7], R. B. Vogelaar[68], C. W. Walter[10,59], D. Wark[41,53],
M. O. Wascko[17], A. Weber[41,53], R. Wendell[57,59], R. J. Wilkes[66], M. J. Wilking[52],
J. R. Wilson[46], T. Xin[23], K. Yamamoto[40], C. Yanagisawa[52,¶], T. Yano[25],
S. Yen[62], N. Yershov[22], M. Yokoyama[60,59,∗], and M. Zito[7]

[1]*University of Bern, Albert Einstein Center for Fundamental Physics, Laboratory for High Energy Physics (LHEP), Bern, Switzerland*
[2]*Boston University, Department of Physics, Boston, MA, USA*
[3]*University of British Columbia, Department of Physics and Astronomy, Vancouver, BC, Canada*
[4]*University of California, Davis, Department of Physics, Davis, CA, USA*
[5]*University of California, Irvine, Department of Physics and Astronomy, Irvine, CA, USA*
[6]*California State University, Department of Physics, Carson, CA, USA*
[7]*IRFU, CEA Saclay, Gif-sur-Yvette, France*
[8]*Chonnam National University, Department of Physics, Gwangju, Korea*
[9]*Dongshin University, Department of Physics, Naju, Korea*
[10]*Duke University, Department of Physics, Durham, NC, USA*
[11]*University of Durham, Science Laboratories, Durham, UK*
[12]*Ecole Polytechnique, IN2P3-CNRS, Laboratoire Leprince-Ringuet, Palaiseau, France*
[13]*University of Edinburgh, School of Physics and Astronomy, Edinburgh, UK*
[14]*ETH Zurich, Institute for Particle Physics, Zurich, Switzerland*
[15]*University of Geneva, Section de Physique, DPNC, Geneva, Switzerland*
[16]*University of Hawaii, Department of Physics and Astronomy, Honolulu, HI, USA*
[17]*Imperial College London, Department of Physics, London, UK*
[18]*INFN Sezione di Bari and Università e Politecnico di Bari, Dipartimento Interuniversitario di Fisica, Bari, Italy*
[19]*INFN Sezione di Napoli and Università di Napoli, Dipartimento di Fisica, Napoli, Italy*
[20]*INFN Sezione di Padova and Università di Padova, Dipartimento di Fisica, Padova, Italy*
[21]*INFN Sezione di Roma, Roma, Italy*
[22]*Institute for Nuclear Research of the Russian Academy of Sciences, Moscow, Russia*
[23]*Iowa State University, Department of Physics and Astronomy, Ames, IA, USA*
[24]*High Energy Accelerator Research Organization (KEK), Tsukuba, Ibaraki, Japan*
[25]*Kobe University, Department of Physics, Kobe, Japan*
[26]*Kyoto University, Department of Physics, Kyoto, Japan*
[27]*Laboratori Nazionali di Frascati, Frascati, Italy*
[28]*Lancaster University, Physics Department, Lancaster, UK*
[29]*University of Liverpool, Department of Physics, Liverpool, UK*
[30]*Los Alamos National Laboratory, NM, USA*
[31]*Louisiana State University, Department of Physics and Astronomy, Baton Rouge, LA, USA*
[32]*University Autonoma Madrid, Department of Theoretical Physics, Madrid, Spain*
[33]*Michigan State University, Department of Physics and Astronomy, East Lansing, MI, USA*
[34]*Miyagi University of Education, Department of Physics, Sendai, Japan*
[35]*Nagoya University, Graduate School of Science, Nagoya, Japan*
[36]*Nagoya University, Kobayashi-Maskawa Institute for the Origin of Particles and the Universe, Nagoya, Japan*
[37]*Nagoya University, Solar-Terrestrial Environment Laboratory, Nagoya, Japan*
[38]*National Centre for Nuclear Research, Warsaw, Poland*
[39]*Okayama University, Department of Physics, Okayama, Japan*
[40]*Osaka City University, Department of Physics, Osaka, Japan*
[41]*Oxford University, Department of Physics, Oxford, UK*

[42]*University of Pittsburgh, Department of Physics and Astronomy, Pittsburgh, PA, USA*

[43]*University of Regina, Department of Physics, Regina, SK, Canada*

[44]*Pontifícia Universidade Católica do Rio de Janeiro, Departamento de Física, Rio de Janeiro, Brazil*

[45]*University of Rochester, Department of Physics and Astronomy, Rochester, NY, USA*

[46]*Queen Mary University of London, School of Physics and Astronomy, London, UK*

[47]*Royal Holloway University of London, Department of Physics, Egham, Surrey, UK*

[48]*Universidade de São Paulo, Instituto de Física, São Paulo, Brazil*

[49]*University of Sheffield, Department of Physics and Astronomy, Sheffield, UK*

[50]*Seoul National University, Department of Physics, Seoul, Korea*

[51]*Seoyeong University, Department of Fire Safety, Gwangju, Korea*

[52]*State University of New York at Stony Brook, Department of Physics and Astronomy, Stony Brook, NY, USA*

[53]*STFC, Rutherford Appleton Laboratory, Harwell Oxford, and Daresbury Laboratory, Warrington, UK*

[54]*Sungkyunkwan University, Department of Physics, Suwon, Korea*

[55]*Research Center for Neutrino Science, Tohoku University, Sendai, Japan*

[56]*University of Tokyo, Earthquake Research Institute, Tokyo, Japan*

[57]*University of Tokyo, Institute for Cosmic Ray Research, Kamioka Observatory, Kamioka, Japan*

[58]*University of Tokyo, Institute for Cosmic Ray Research, Research Center for Cosmic Neutrinos, Kashiwa, Japan*

[59]*University of Tokyo, Kavli Institute for the Physics and Mathematics of the Universe (WPI), Todai Institutes for Advanced Study, Kashiwa, Chiba, Japan*

[60]*University of Tokyo, Department of Physics, Tokyo, Japan*

[61]*Tokyo Institute of Technology, Department of Physics, Tokyo, Japan*

[62]*TRIUMF, Vancouver, BC, Canada*

[63]*University of Toronto, Department of Physics, Toronto, ON, Canada*

[64]*University of Warsaw, Faculty of Physics, Warsaw, Poland*

[65]*University of Warwick, Department of Physics, Coventry, UK*

[66]*University of Washington, Department of Physics, Seattle, WA, USA*

[67]*University of Winnipeg, Department of Physics, Winnipeg, MB, Canada*

[68]*Virginia Tech, Center for Neutrino Physics, Blacksburg, VA, USA*

[69]*Wroclaw University, Faculty of Physics and Astronomy, Wroclaw, Poland*

[70]*York University, Department of Physics and Astronomy, Toronto, ON, Canada*

[*]E-mail: masashi@phys.s.u-tokyo.ac.jp

. . . .

Hyper-Kamiokande will be a next-generation underground water Cherenkov detector with a total (fiducial) mass of 0.99 (0.56) million metric tons, approximately 20 (25) times larger than that of Super-Kamiokande. One of the main goals of Hyper-Kamiokande is the study of CP asymmetry in the lepton sector using accelerator neutrino and anti-neutrino beams. In this paper, the physics potential of a long-baseline neutrino experiment using the Hyper-Kamiokande detector and a neutrino beam from the J-PARC proton synchrotron is presented. The analysis uses the framework and systematic uncertainties derived from the ongoing T2K experiment. With a total exposure of $7.5\,\mathrm{MW} \times 10^7$ s integrated proton beam power (corresponding to 1.56×10^{22} protons on target with a 30 GeV proton beam) to a $2.5°$ off-axis neutrino beam, it is expected that the leptonic CP phase δ_{CP} can be determined to better than 19 degrees for all possible values of δ_{CP}, and CP violation can be established with a statistical significance of more than 3σ (5σ) for 76% (58%) of the δ_{CP} parameter space. Using both ν_e appearance and ν_μ disappearance data, the expected 1σ uncertainty of $\sin^2 \theta_{23}$ is 0.015(0.006) for $\sin^2 \theta_{23} = 0.5(0.45)$.

. . . .

Subject Index   C03, C04, C32

1. Introduction

The discovery of neutrino oscillations by the Super-Kamiokande (Super-K) experiment in 1998 [1] opened a new window to explore physics beyond the Standard Model (BSM). Evidence of neutrino oscillations is one of the most convincing experimental proofs known today for the existence of BSM physics at work. The mixing parameters of neutrinos were found to be remarkably different from those of quarks, which suggests the presence of an unknown flavor symmetry waiting to be explored. The extremely small masses of neutrinos compared with those of their charged partners lead to the preferred scenario of a seesaw mechanism [2–5], in which small neutrino masses are a reflection of the ultra-high-energy scale of BSM physics.

Furthermore, a theoretical framework called leptogenesis points to the intriguing possibility that CP asymmetries related to flavor mixing among the three generations of neutrinos may have played an important role in creating the observed matter–antimatter asymmetry in the universe [6]. This makes a study of the full picture of neutrino masses and mixings and the measurement of the CP asymmetry in the neutrino sector among the most important and urgent subjects in today's elementary particle physics world.

CP asymmetry in the neutrino sector arising from the presence of the phase that corresponds to the Kobayashi–Maskawa phase [7] in the quark sector can only be seen if all the three mixing angles governing neutrino oscillations differ from zero. The Super-K detector has successfully measured all three angles. The angle θ_{23} was first measured in atmospheric neutrino observations [1], θ_{12} was constrained in solar neutrino observations [8] (together with another water Cherenkov detector SNO [9]), and the evidence of nonzero θ_{13} was found by T2K [10], which used Super-K as the far detector. In 2013, T2K established $\nu_\mu \rightarrow \nu_e$ oscillation with $7.3\,\sigma$ significance, leading the way towards CP violation measurements in neutrinos [11] in combination with precise measurements of θ_{13} by reactor neutrino experiments [12–14]. The highly successful Super-K program indicates that Hyper-Kamiokande (Hyper-K) is well placed to discover CP violation.

In this paper, the physics potential of a long-baseline neutrino experiment using the Hyper-Kamiokande detector and a neutrino beam from the J-PARC proton synchrotron is presented.

The Hyper-K detector is designed as a next-generation underground water Cherenkov detector that serves as a far detector of a long-baseline neutrino oscillation experiment for the J-PARC neutrino beam and as a detector capable of observing proton decays, atmospheric and solar neutrinos, and neutrinos from other astrophysical origins. The baseline design of Hyper-K is based on the well proven technologies employed and tested at Super-K. Hyper-K consists of two cylindrical tanks lying side-by-side, the outer dimensions of each tank being 48 (W) × 54 (H) × 250 (L) m^3. The total (fiducial) mass of the detector is 0.99 (0.56) million metric tons, which is about 20 (25) times larger than that of Super-K. A proposed location for Hyper-K is about 8 km south of Super-K (and 295 km away from J-PARC) and 1750 meters water equivalent (or 648 m of rock) deep. The inner detector region is viewed by 99 000 20 inch PMTs, corresponding to a PMT density of 20% photocathode coverage (the same as the second phase of Super-K). A schematic view of the Hyper-K detector is illustrated in Fig. 1.

In addition to the long-baseline neutrino oscillation experiment that is the main focus of this paper, Hyper-K will provide a rich program in a wide range of science [15]. The scope of the project includes observation of atmospheric and solar neutrinos, proton decays, and neutrinos from other astrophysical origins. The physics potential of Hyper-K is summarized in Table 1.
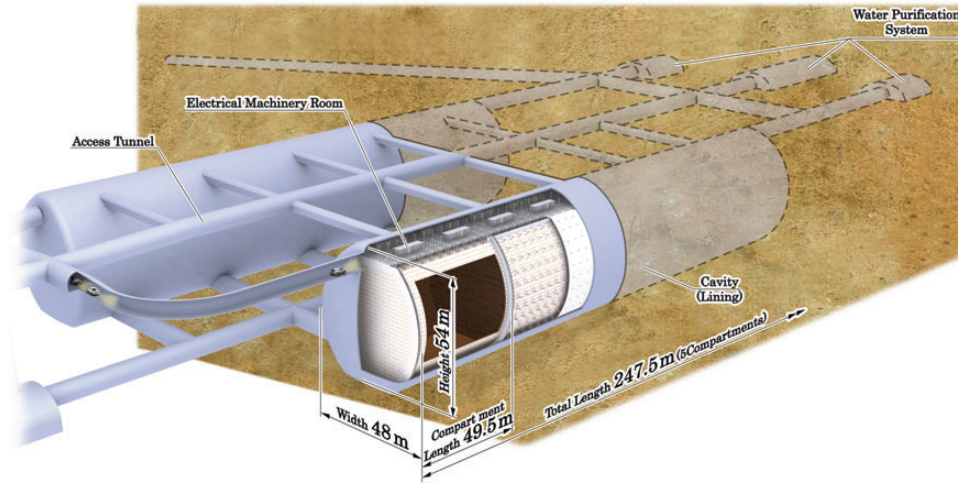
Fig. 1. Schematic view of the Hyper-Kamiokande detector.

Table 1. Physics targets and expected sensitivities of the Hyper-Kamiokande experiment, based on the study shown in Ref. [15] except for the long-baseline experiment that is described in this paper. Improvement is expected with further optimization of the detector design and development of reconstruction/analysis tools. Also, only selected values are listed; e.g., other channels will be accessible for nucleon decays.

Physics target	Sensitivity	Conditions
Neutrino study w/ J-PARC ν		$7.5\,\mathrm{MW} \times 10^7\,\mathrm{s}$
$-\,CP$ phase precision	$<19°$	@ $\sin^2 2\theta_{13} = 0.1$, mass hierarchy known
$-\,CPV$ discovery coverage	76% (3σ), 58% (5σ)	@ $\sin^2 2\theta_{13} = 0.1$, mass hierarchy known
$-\,\sin^2\theta_{23}$	± 0.015	1σ @ $\sin^2\theta_{23} = 0.5$
Atmospheric neutrino study		10 yr observation
$-$ MH determination	$>3\sigma$ CL	@ $\sin^2\theta_{23} > 0.4$
$-\,\theta_{23}$ octant determination	$>3\sigma$ CL	@ $\sin^2\theta_{23} < 0.46$ or $\sin^2\theta_{23} > 0.56$
Nucleon decay searches		10 yr data
$-\, p \to e^+ + \pi^0$	1.3×10^{35} yr (90% CL UL) 5.7×10^{34} yr (3σ discovery)	
$-\, p \to \bar{\nu} + K^+$	3.2×10^{34} yr (90% CL UL) 1.2×10^{34} yr (3σ discovery)	
Astrophysical neutrino sources		
$-\,^8$B ν from Sun	200 ν/day	7.0 MeV threshold (total energy) w/ osc.
$-$ Supernova burst ν	170 000–260 000 ν 30–50 ν	@ Galactic center (10 kpc) @ M31 (Andromeda galaxy)
$-$ Supernova relic ν	830 ν/10 yr	
$-$ WIMP annihilation at Sun (σ_{SD}: WIMP–proton spin-dependent cross section)	$\sigma_{SD} = 10^{-39}$ cm^2	5 yr observation @ $M_{\mathrm{WIMP}} = 10$ GeV, $\chi\chi \to b\bar{b}$ dominant
	$\sigma_{SD} = 10^{-40}$ cm^2	@ $M_{\mathrm{WIMP}} = 100$ GeV, $\chi\chi \to W^+ W^-$ dominant

2. Neutrino oscillations and CP violation

2.1. *Neutrino oscillations in the three-flavor framework*

Throughout this paper, unless stated otherwise, we consider the standard three-flavor neutrino framework. The 3×3 unitary matrix U that describes the mixing of neutrinos [16] (that is often referred to as the Maki–Nakagawa–Sakata–Pontecorvo (MNSP) or Maki–Nakagawa–Sakata (MNS) [16,17] matrix) relates the flavor and mass eigenstates of neutrinos:

$$\nu_\alpha = \sum_{i=1}^{3} U_{\alpha i} \nu_i, \quad (\alpha = e, \mu, \tau), \tag{1}$$

where $\nu_\alpha (\alpha = e, \mu, \tau)$ and $\nu_i (i = 1, 2, 3)$ denote, respectively, flavor and mass eigenstates of neutrinos. Using the standard parametrization, which can be found, e.g., in Ref. [18], U can be expressed as

$$U = \begin{pmatrix} 1 & 0 & 0 \\ 0 & c_{23} & s_{23} \\ 0 & -s_{23} & c_{23} \end{pmatrix} \begin{pmatrix} c_{13} & 0 & s_{13}e^{-i\delta_{CP}} \\ 0 & 1 & 0 \\ -s_{13}e^{i\delta_{CP}} & 0 & c_{13} \end{pmatrix} \begin{pmatrix} c_{12} & s_{12} & 0 \\ -s_{12} & c_{12} & 0 \\ 0 & 0 & 1 \end{pmatrix}$$

$$\times \begin{pmatrix} 1 & 0 & 0 \\ 0 & e^{i\frac{\alpha_{21}}{2}} & 0 \\ 0 & 0 & e^{i\frac{\alpha_{31}}{2}} \end{pmatrix} \tag{2}$$

where $c_{ij} \equiv \cos\theta_{ij}$, $s_{ij} \equiv \sin\theta_{ij}$, and δ_{CP}—often called the Dirac CP phase—is the Kobayashi–Maskawa-type CP phase [7] in the lepton sector. On the other hand, the two phases, α_{21} and α_{31}—often called Majorana CP phases—exist only if neutrinos are of Majorana type [19–21]. While the Majorana CP phases cannot be observed in neutrino oscillation, they can be probed by lepton-number-violating processes such as neutrinoless double beta decay.

In vacuum, the oscillation probability of $\nu_\alpha \to \nu_\beta$ ($\alpha, \beta = e, \mu, \tau$) for ultrarelativistic neutrinos is given by

$$P(\nu_\alpha \to \nu_\beta) = \left| \sum_{i=1}^{3} U_{\alpha i}^* U_{\beta i} e^{-i\frac{m_i^2}{2E_\nu}L} \right|^2$$

$$= \delta_{\alpha\beta} - 4 \sum_{i>j} \Re\left(U_{\alpha i}^* U_{\alpha j} U_{\beta i} U_{\beta j}^* \right) \sin^2\left(\frac{\Delta m_{ij}^2}{4E_\nu} L \right)$$

$$+ 2 \sum_{i>j} \Im\left(U_{\alpha i}^* U_{\alpha j} U_{\beta i} U_{\beta j}^* \right) \sin\left(\frac{\Delta m_{ij}^2}{2E_\nu} L \right), \tag{3}$$

where E_ν is the neutrino energy, L is the baseline, and $\Delta m_{ij}^2 \equiv m_i^2 - m_j^2$ ($i, j = 1, 2, 3$) are the mass-squared differences with m_i and m_j being the neutrino masses. For the CP conjugate channel, $\bar{\nu}_\alpha \to \bar{\nu}_\beta$, the same expression in Eq. (3) holds, but the matrix U is replaced by its complex conjugate (or equivalently $\delta_{CP} \to -\delta_{CP}$ in Eq. (2)), resulting in the third term in Eq. (3) switching sign. For neutrinos traveling inside matter, coherent forward scattering induces an asymmetry between the oscillation probabilities of neutrinos and anti-neutrinos supplementary to the intrinsic CP violation.

The magnitude of the CP violation in neutrino oscillation can be characterized by the difference in probabilities between neutrino and anti-neutrino channels, which, in vacuum, is given by [22,23]

$$\Delta P_{\alpha\beta} \equiv P(\nu_\alpha \to \nu_\beta) - P(\bar{\nu}_\alpha \to \bar{\nu}_\beta) = 16 J_{\alpha\beta} \sin\Delta_{21} \sin\Delta_{32} \sin\Delta_{31}, \tag{4}$$

and

$$J_{\alpha\beta} \equiv \Im\left(U_{\alpha 1} U_{\alpha 2}^* U_{\beta 1}^* U_{\beta 2}\right) = \pm J_{CP}, \quad J_{CP} \equiv s_{12} c_{12} s_{23} c_{23} s_{13} c_{13}^2 \sin\delta_{CP} \tag{5}$$

with positive (negative) sign for (anti-)cyclic permutation of the flavor indices e, μ, and τ. The parameter J_{CP} is the lepton analogue of the CP-invariant factor for quarks, the unique and phase-convention-independent measure for CP violation [24]. Using the current best-fitted values of mixing parameters [25], we get $J_{CP} \simeq 0.034 \sin\delta_{CP}$, or

$$\Delta P_{\alpha\beta} \simeq \pm 0.55 \sin\delta_{CP} \sin\Delta_{21} \sin\Delta_{32} \sin\Delta_{31}. \tag{6}$$

Thus, large CP violation effects are possible in the neutrino oscillation.

In general, it is considered that the CP violation in the neutrino sector that can be observed in the low-energy regime, namely, in neutrino oscillation, does not directly imply the CP violation required at high energy for successful leptogenesis in the early universe. It has been discussed, however, that they could be related to each other, and the CP-violating phase in the MNS matrix could also be responsible for the generation of the observed baryon asymmetry through leptogenesis in some scenarios. For example, in Refs. [26,27], in the context of the seesaw mechanism, it has been pointed out that, assuming the hierarchical mass spectrum for right-handed Majorana neutrinos with the lightest mass being $\lesssim 5 \times 10^{12}$ GeV, the observed baryon asymmetry could be generated through leptogenesis if $|\sin\theta_{13} \sin\delta_{CP}| \gtrsim 0.1$, which is compatible with the current neutrino data. Hence, measurement of CP asymmetry in neutrino oscillations may provide a clue for understanding the origin of the matter–antimatter asymmetry of the universe.

Since there are only three neutrinos, only two mass-squared differences, e.g., Δm_{21}^2 and Δm_{31}^2, are independent. Therefore, for a given energy and baseline, there are six independent parameters, namely, three mixing angles, one CP phase, and two mass-squared differences, to describe neutrino oscillations. Among these six parameters, θ_{12} and Δm_{21}^2 have been measured by solar [9,28,29] and reactor [30–32] neutrino experiments. The parameters θ_{23} and $|\Delta m_{32}^2|$ (only its absolute value) have been measured by atmospheric [33,34] and accelerator [35–38] neutrino experiments. Reactor experiments have also started to measure the atmospheric mass-squared difference, $|\Delta m_{31}^2|$, though the uncertainty is still large [12]. Recently, (θ_{13}) has also been measured by accelerator [10,11,39,40] and reactor experiments [12–14,41,42]. The relatively large value of θ_{13} opens a window to explore the CP phase (δ_{CP}) and the mass hierarchy (the sign of Δm_{31}^2) using neutrino oscillation.

2.2. Physics case with $\nu_\mu \to \nu_e$ oscillation

The oscillation probability from ν_μ to ν_e in accelerator experiments is expressed, to the first order of the matter effect, as follows [43]:

$$
\begin{aligned}
P(\nu_\mu \to \nu_e) = {} & 4 c_{13}^2 s_{13}^2 s_{23}^2 \cdot \sin^2\Delta_{31} \\
& + 8 c_{13}^2 s_{12} s_{13} s_{23} \left(c_{12} c_{23} \cos\delta_{CP} - s_{12} s_{13} s_{23}\right) \cdot \cos\Delta_{32} \cdot \sin\Delta_{31} \cdot \sin\Delta_{21} \\
& - 8 c_{13}^2 c_{12} c_{23} s_{12} s_{13} s_{23} \sin\delta_{CP} \cdot \sin\Delta_{32} \cdot \sin\Delta_{31} \cdot \sin\Delta_{21} \\
& + 4 s_{12}^2 c_{13}^2 \left(c_{12}^2 c_{23}^2 + s_{12}^2 s_{23}^2 s_{13}^2 - 2 c_{12} c_{23} s_{12} s_{23} s_{13} \cos\delta_{CP}\right) \cdot \sin^2\Delta_{21} \\
& - 8 c_{13}^2 s_{13}^2 s_{23}^2 \cdot \frac{aL}{4E_\nu}\left(1 - 2 s_{13}^2\right) \cdot \cos\Delta_{32} \cdot \sin\Delta_{31} \\
& + 8 c_{13}^2 s_{13}^2 s_{23}^2 \frac{a}{\Delta m_{31}^2}\left(1 - 2 s_{13}^2\right) \cdot \sin^2\Delta_{31},
\end{aligned}
\tag{7}
$$

where Δ_{ij} is $\Delta m_{ij}^2 L/4E_\nu$, and $a = 2\sqrt{2}G_F n_e E_\nu = 7.56 \times 10^{-5} \left[\text{eV}^2\right] \times \rho \left[\text{g/cm}^3\right] \times E_\nu \left[\text{GeV}\right]$. The corresponding probability for a $\bar{\nu}_\mu \to \bar{\nu}_e$ transition is obtained by replacing $\delta_{CP} \to -\delta_{CP}$ and $a \to -a$. The third term, containing $\sin \delta_{CP}$, is the CP-violating term that flips sign between ν and $\bar{\nu}$ and thus introduces CP asymmetry if $\sin \delta_{CP}$ is nonzero. The last two terms are due to the matter effect. Those terms that contain a change their sign depending on the mass hierarchy. As seen from the definition of a, the amount of asymmetry due to the matter effect is proportional to the neutrino energy at a fixed value of L/E_ν. A direct test of CP violation, in a model-independent way, is possible by measuring both neutrino and anti-neutrino appearance probabilities. If the mass hierarchy is not known, the sensitivity of CP violation is affected by the presence of the matter effect. However, the mass hierarchy could be determined by the atmospheric neutrino measurement in Hyper-K and several measurements by other experiments.

The currently measured value of θ_{23} is consistent with maximal mixing, $\theta_{23} \approx \pi/4$ [38,44,45]. It is of great interest to determine if $\sin^2 2\theta_{23}$ is maximal or not, and, if not, if θ_{23} is less or greater than $\pi/4$, as it could constrain models of neutrino mass generation [46–51]. When we measure θ_{23} with the survival probability $P\left(\nu_\mu \to \nu_\mu\right)$, which is proportional to $\sin^2 2\theta_{23}$ to first order,

$$P\left(\nu_\mu \to \nu_\mu\right) \simeq 1 - 4c_{13}^2 s_{23}^2 \left[1 - c_{13}^2 s_{23}^2\right] \sin^2 \left(\Delta m_{32}^2 L/4E_\nu\right) \tag{8}$$

$$\simeq 1 - \sin^2 2\theta_{23} \sin^2 \left(\Delta m_{32}^2 L/4E_\nu\right), \quad \text{(for } c_{13} \simeq 1) \tag{9}$$

there is an octant ambiguity: either $\theta_{23} \leq 45°$ (in the first octant) or $\theta_{23} > 45°$ (in the second octant). By combining the measurement of $P(\nu_\mu \to \nu_e)$, the θ_{23} octant can be determined.

2.3. Anticipated neutrino physics landscape in the 2020s and uniqueness of this experiment

Before Hyper-K commences data taking in $\sim$2025, we expect that a number of ongoing and planned neutrino experiments as well as cosmological observations will advance our understanding of neutrino physics. In addition to accelerator and reactor experiments, Super-K will provide precise measurements of neutrino oscillation parameters from atmospheric neutrino observations, and will look for the mass hierarchy and the octant of θ_{23}. Cosmological observations will provide the information on neutrino masses. An observation of neutrinoless double β decay in the next 10 years would be evidence that the neutrino is a Majorana particle with the inverted mass hierarchy. Following this progress, we definitely need a new experiment to discover CP violation in neutrinos, and to unambiguously establish the mass hierarchy and θ_{23} octant. For these purposes, we propose the Hyper-K experiment with the J-PARC neutrino beam.

The Hyper-K experiment will have several unique advantages.

○ The experiment will have high statistics of neutrino events thanks to the large fiducial mass and the high-power J-PARC neutrino beam.
○ The relatively short baseline among the proposed long-baseline experiments results in a small ambiguity from the matter effect.
○ The experiment will operate in the same beamline as T2K with the same off-axis configuration. The features of the neutrino beam and the operation of the high-power beam are well understood.
○ The systematic errors are already well understood based on Super-K and T2K, allowing reliable extrapolations.

With these features, Hyper-K will be one of the most sensitive experiments to probe neutrino CP violation, as we present in this paper.

3.   Experimental setup

3.1.   *J-PARC accelerator and neutrino beamline*

An intense and high-quality neutrino beam is key to the success of a long-baseline neutrino oscillation experiment. J-PARC (Japan Proton Accelerator Research Complex) is one of the world's leading facilities in neutrino physics, currently providing a beam for the T2K experiment. We will utilize the full potential of this existing facility with future increase of the beam power to the designed value of 750 kW and beyond.

The J-PARC accelerator cascade [52] consists of a normal-conducting LINAC as an injection system, a rapid cycling synchrotron (RCS), and a main ring synchrotron (MR). In the fast extraction mode operation, MR has achieved 1.24×10^{14} protons per pulse (ppp) beam intensity, which is a world record for extracted ppp for any synchrotron. The corresponding beam power is 240 kW. The upgrade scenario of the J-PARC accelerator [53] is being implemented to reach the designed power of 750 kW in forthcoming years, with a typical planned parameter set as listed in Table 2. This will double the current repetition rate by (i) replacing the magnet power supplies, (ii) replacing the RF system, and (iii) upgrading injection/extraction devices. The designed power of 750 kW will be achieved well before Hyper-K starts data taking. Furthermore, conceptual studies on how to realize 1–2 MW beam powers and even beyond, such as by raising the RCS top energy, enlarging the MR aperture, or inserting an "emittance-damping" ring between the RCS and MR, are now underway [54].

Figure 2 shows an overview of the neutrino experimental facility [55,56]. The primary beamline guides the extracted proton beam to a production target/pion-focusing horn system in a target station. The pions decay into muons and neutrinos during their flight in a 110 m-long decay volume. A graphite beam dump is installed at the end of the decay volume, and muon monitors downstream of the beam dump monitor the muon profile. A near neutrino detector complex is situated 280 m downstream of the target to monitor neutrinos at production. To generate a narrow-band neutrino beam, the beamline utilizes an off-axis beam configuration [57], with the capability of varying the off-axis angle in a range from 2.0° to 2.5°. The latter value has been used for the T2K experiment and is also assumed for the proposed project. The centerline of the beamline extends 295 km to the west, passing midway between Tochibora (Hyper-K candidate site) and Mozumi (where Super-K is located), so that both sites have identical off-axis angles.

Based on the considerable experience gained on the path to achieving 240 kW beam power operation, improvement plans to realize 750 kW operation, such as improving the activated air confinement in the target station and expanding the facilities for the treatment of activated water, are being implemented and/or proposed. Table 3 gives a summary of the acceptable beam power and/or achievable parameters for each beamline component [58], after the proposed improvements in forthcoming years.

3.2.   *Near detectors*

The accelerator neutrino event rate observed at Hyper-K depends on the oscillation probability, neutrino flux, neutrino interaction cross section, detection efficiency, and the detector fiducial mass of Hyper-K. To extract estimates of the oscillation parameters from data, one must model the neutrino flux, cross section, and detection efficiency with sufficient precision. In the case of the neutrino cross

Table 2. Planned parameters of the J-PARC main ring for fast extraction. Numbers in parentheses are those achieved up to May 2013.

Parameter	Value
Circumference (m)	1567.5
Kinetic energy (GeV)	30
Beam intensity (ppp)	2.0×10^{14} (1.24×10^{14})
(ppb)	2.5×10^{13} (1.57×10^{13})
Harmonic number	9
Number of bunches per spill	8
Spill width (μs)	~5
Bunch full width at extraction (ns)	~50
Maximum RF voltage (kV)	560 (280)
Repetition period (s)	1.28 (2.48)
Beam power (kW)	750 (240)
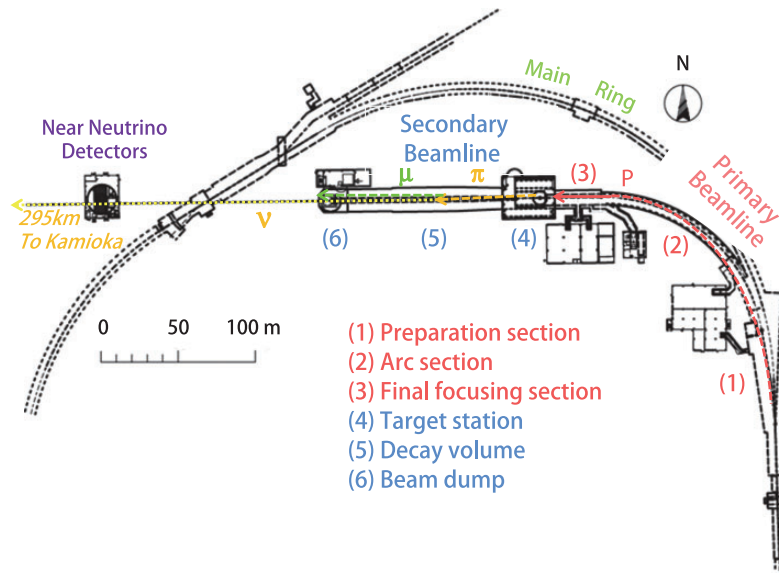
Fig. 2. The neutrino experimental facility (neutrino beamline) at J-PARC.

section, the model must describe the exclusive differential cross section that includes the dependence on the incident neutrino energy, E_ν, the kinematics of the outgoing lepton, p_l and θ_l, and the kinematics of final-state hadrons and photons. In our case, the neutrino energy is inferred from the lepton kinematics, while the modeling of reconstruction efficiencies depends on the hadronic final state as well.

The neutrino flux and cross-section models can be constrained by data collected at near detectors, situated close enough to the neutrino production point so that oscillation effects are negligible. Our approach to using near-detector data will build on the experience of T2K while considering new near detectors that may address important uncertainties in the neutrino flux or cross-section modeling.

The conceptual design of the near detectors is being developed based on the physics sensitivity studies described in Sect. 4. In this section, we present basic considerations on the near-detector requirements and conceptual designs. More concrete requirements and a detector design will be presented in the future.

Table 3. Acceptable beam power and achievable parameters for each beamline component [58]. Limitations as of May 2013 are also given in parentheses.

Component	Beam power/parameter
Target	3.3×10^{14} ppp
Beam window	3.3×10^{14} ppp
Horn	
Cooling for conductors	2 MW
Stripline cooling	1–2 MW (400 kW)
Hydrogen production	1–2 MW (300 kW)
Horn current	320 kA (250 kA)
Power supply repetition	1 Hz (0.4 Hz)
Decay volume	4 MW
Hadron absorber/beam dump	3 MW
Water cooling facilities	∼2 MW (750 kW)
Radiation shielding	4 MW (750 kW)
Radioactive air leakage to the target station ground floor	∼2 MW (500 kW)
Radioactive cooling water treatment	∼2 MW (600 kW)

We assume the use of T2K near detectors [55], INGRID and ND280, possibly with an upgrade. The INGRID detector [59] consists of 16 iron-scintillator modules configured in a cross pattern centered on the beam axis 280 m downstream of the T2K target. The rate of interactions in each module is measured and a profile is constructed to constrain the neutrino beam direction. The ND280 off-axis detector is located 280 m downstream of the T2K target as well, but at an angle of 2.5 degrees away from the beam direction. It consists of the P0D π^0 detector [60], time projection chambers (TPCs) [61], fine-grain scintillator bar detectors (FGDs) [62] and surrounding electromagnetic calorimeters (ECALs) [63]. The detectors are immersed in a 0.2 T magnetic field and the magnetic yoke is instrumented with plastic scintillator panels for muon range detection [64]. The magnetic field allows for momentum measurement and sign selection of charged particles. The magnetization of ND280 is particularly important for operation in anti-neutrino mode where the neutrino background is large. In that case, ND280 is able to separate the "right-sign" μ^+ from the "wrong-sign" μ^-. The P0D and FGDs act as the neutrino targets, while the TPCs provide measurements of momentum and ionizing energy loss for particle identification. The P0D and one of the FGDs include passive water layers that allow for neutrino interaction rate measurements on the same target as Super-K. ND280 has been employed to measure the rates of charged-current (CC) ν_μ and ν_e interactions, as well as neutral-current (NC) π^0 interactions.

The T2K Collaboration is in the process of discussing various upgrade possibilities at the ND280 site [65]. These include the deployment of heavy water (D_2O) within the passive water targets in FGD2 that would allow the extraction of neutrino interaction properties on the quasi-free neutron in deuterium via a subtraction with data taken with light water H_2O. The use of a water-based liquid scintillator (WbLS) developed at BNL [66] is being explored in the context of a tracking detector with comparable or finer granularity than the FGD to allow the detailed reconstruction of the hadronic system emerging from the neutrino interactions or a larger detector with coarser segmentation that would allow high-statistics studies. Either would significantly enhance the study of neutrino interactions on water by reducing the reliance on subtraction and enhancing the reconstruction capabilities relative to the currently deployed passive targets. Finally, a high-pressure TPC that can contain various noble gases (He, Ne, Ar) to serve both as the target and tracking medium is being studied. Such a detector would allow the ultimate resolution of the particles emitted from the target nucleus while

allowing a study of the *A*-dependence of the cross sections and final-state interactions to rigorously test models employed in neutrino event generators.

Since many of the uncertainties on the modeling of neutrino interactions arise from uncertainties on nuclear effects, the ideal near detector should include the same nuclear targets as the far detector. In T2K near detectors, the P0D [60] and FGD [62] detectors include passive water layers; however, extracting water-only cross sections requires complicated analyses that subtract out the interactions on other materials in the detectors. An alternative approach is to build a water Cherenkov (WC) near detector to measure the cross section on H_2O directly and with no need for a subtraction analysis. This approach was taken by K2K [35] and was proposed for T2K [67]. The MiniBooNE experiment has also employed a mineral-oil Cherenkov detector at a short baseline to great success [68]. A WC near-detector design is largely guided by two requirements:

(1) The detector should be large enough to contain muons up to the momentum of interest for measurements at the far detector, and to provide sufficient radiation length for detection of gamma rays.
(2) The detector should be far enough from the neutrino production point so that there is minimal pile-up of interactions in the same beam timing bunch.

These requirements lead to designs for kiloton-size detectors located at intermediate distances, 1–2 km from the target, for the J-PARC neutrino beam.

The main disadvantage of the WC detector is the inability to separate positively and negatively charged leptons, and hence anti-neutrino and neutrino interactions. This ability is especially important for a CP asymmetry measurement where the wrong sign contribution to the neutrino flux should be well understood. Hence, the WC detector will most likely be used in conjunction with a magnetized tracking detector such as ND280. Recent developments in the addition of gadolinium (Gd) [69] and water-based liquid scintillator (WbLS) compounds [66] to water do raise the possibility of separating neutrino and anti-neutrino interactions by detecting the presence of neutrons or protons in the final state.

Two conceptual designs for possible intermediate WC detectors have been studied. Unoscillated Spectrum (TITUS) is a 2 kiloton WC detector located about 2 km from the target at the same off-axis angle as the far detector. At this baseline the detector sees fluxes for the neutral-current and ν_e backgrounds that are nearly identical to the Hyper-K fluxes. The detector geometry and the presence of a muon range detector are optimized to detect the high-momentum tail of the muon spectrum. The use of Gd in TITUS to separate neutrino and anti-neutrino interactions is being studied. The νPRISM detector is located 1 km from the target and is 50 m tall, covering a range of off-axis angles from 1–4 degrees. The νPRISM detector sees a range of neutrino spectra, peaking at energies from 0.4 to 1.0 GeV depending on the off-axis angle. The purpose of νPRISM is to use these spectra to better probe the relationship between the incident neutrino energy and final-state lepton kinematics, a part of the interaction model with larger uncertainties arising from nuclear effects.

3.3. *Hyper-Kamiokande*

Hyper-Kamiokande is to be the third-generation water Cherenkov detector in Kamioka, designed for a wide variety of neutrino studies and nucleon decay searches. Its total (fiducial) water mass of one (0.56) million tons would be approximately 20 (25) times larger than that of Super-Kamiokande. Table 4 summarizes the baseline design parameters of the Hyper-K detector.

**Table 4.** Parameters of the Hyper-Kamiokande baseline design.

Detector type		Ring-imaging water Cherenkov detector
Candidate site	Address	Tochibora mine
		Kamioka town, Gifu, JAPAN
	Lat.	36°21′20.105″N[†]
	Long.	137°18′49.137″E[†]
	Alt.	508 m
	Overburden	648 m rock
		(1750 m water equivalent)
	Cosmic-ray muon flux	$\sim 8 \times 10^{-7}\,\mathrm{s}^{-1}\,\mathrm{cm}^{-2}$
	Off-axis angle for the J-PARC ν	2.5° (same as Super-K)
	Distance from the J-PARC	295 km (same as Super-K)
Detector geometry	Total water mass	0.99 megaton
	Inner detector (fiducial) mass	0.74 (0.56) megaton
	Outer detector mass	0.2 megaton
Photo-sensors	Inner detector	99 000 20 inch ϕ PMTs
		20% photo-coverage
	Outer detector	25 000 8 inch ϕ PMTs
Water quality	Light attenuation length	>100 m @ 400 nm
	Rn concentration	<1 mBq/m^3

[†]World geographical coordination system.

In the baseline design, the Hyper-K detector is composed of two separate caverns, as shown in Fig. 1, each having an egg-shaped cross section 48 meters wide, 54 meters tall, and 250 meters long, as shown in Figs. 3 and 4. The welded polyethylene tanks are filled up to a depth of 48 m with ultra-pure water: the total water mass equals 0.99 million tons.

Each tank will be optically separated by segmentation walls located every 49.5 m to form 5 (in total 10) compartments, as shown in Fig. 4, such that event triggering and event reconstruction can be performed in each compartment separately and independently. Because the compartment dimension of 50 m is comparable with that of Super-K (36 m) and is shorter than the typical light attenuation length in water achieved by the Super-K water filtration system (>100 m @ 400 nm), we expect that the detector performance of Hyper-K for beam and atmospheric neutrinos will be effectively the same as that of Super-K.

The water in each compartment is further optically separated into three regions. The inner region has a barrel shape of 42 m in height and width, and 48.5 m in length, and is viewed by an inward-facing array of 20 inch diameter photomultiplier tubes (PMTs). The entire array consists of 99 000 Hamamatsu R3600 PMTs, uniformly surrounding the region and giving a photocathode coverage of 20%. The PMT type, size, and number density are subject to optimization. We have also been developing new photosensors as possible alternative options to the R3600, such as a PMT with a box-and-line dynode and a hybrid photo-detector (HPD), both with a high-quantum-efficiency photocathode. An outer region completely surrounds the 5 (in total 10) inner regions and is equipped with 25 000 8 inch diameter PMTs. This region is 2 m thick at the top, bottom, and barrel sides, except at both ends of each cavern, where the outer region is larger than 2 m due to rock engineering considerations. A primary function of the outer detector is to reject entering cosmic-ray muon backgrounds and to help in identifying nucleon decays and neutrino interactions occurring in the inner
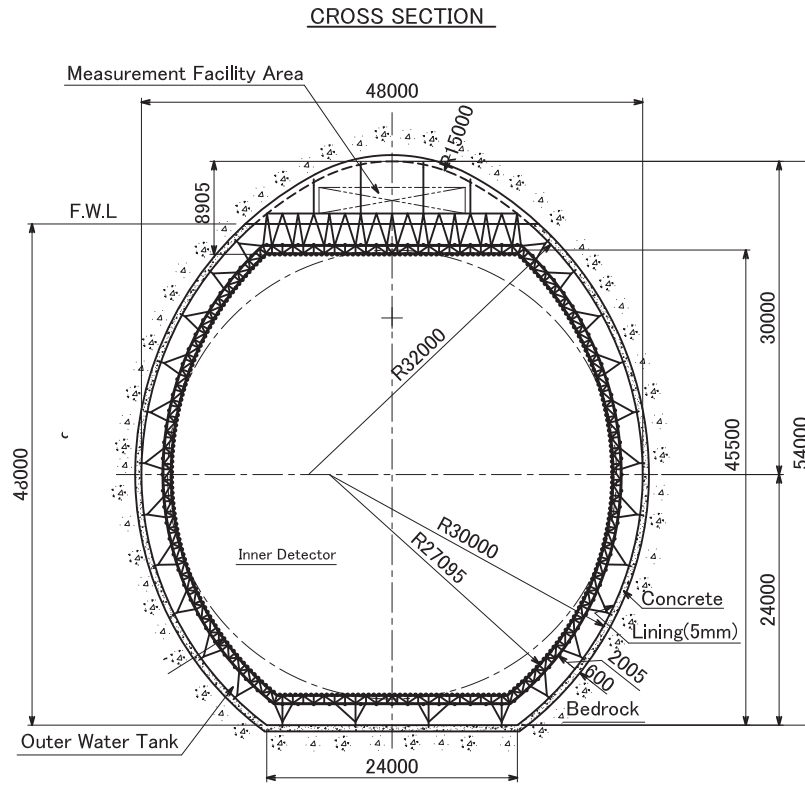
CROSS SECTION

**Fig. 3.** Cross-section view of the Hyper-Kamiokande detector.

detector. The middle region or dead space is an uninstrumented, 0.9 m thick shell between the inner and outer detector volumes where the stainless steel PMT support structure is located. The borders of both the inner and outer regions are lined with opaque sheets. This dead space, along with the outer region, acts as a shield against radioactivity from the surrounding rock. The total water mass of the inner region is 0.74 million tons and the total fiducial mass is 10 times $0.056 = 0.56$ million tons. The fiducial volume is defined as the region formed by a virtual boundary located 2 m away from the inner PMT plane.

The estimated cosmic-ray muon rate around the Hyper-K detector candidate site is $\sim 8 \times 10^{-7}$ $s^{-1}\,cm^{-2}$, which is roughly 5 times larger than the flux at Super-K's location ($\sim 1.5 \times 10^{-7}\,s^{-1}\,cm^{-2}$). The expected deadtime due to these muons is less than 1% and is negligible for long-baseline experiments, as well as nucleon decay searches and atmospheric neutrino studies.

Water is the target material and signal-sensitive medium of the detector, and thus its quality directly affects the physics sensitivity. In Super-Kamiokande the water purification system has been continually modified and improved over the course of two decades. As a result, the transparency is now kept above 100 m and is very stable, and the radon concentration in the tank is held below $1\,mBq/m^3$. Following this success, the Hyper-Kamiokande water system has been designed based on the current Super-Kamiokande water system with scaling-up of the process speeds to $1200\,m^3$/hour for water circulation and $400\,m^3$/hour for radon free air generation. With these systems, the water quality in Hyper-Kamiokande is expected to be the same as that in Super-Kamiokande. Adding dissolved gadolinium sulfate for efficient tagging of neutrons has been studied as an option to enhance the Hyper-K physics capability. The feasibility of adding Gd to Super-K [69] is now being studied with the EGADS (Evaluating Gadolinium's Action on Detector Systems) project in Kamioka.
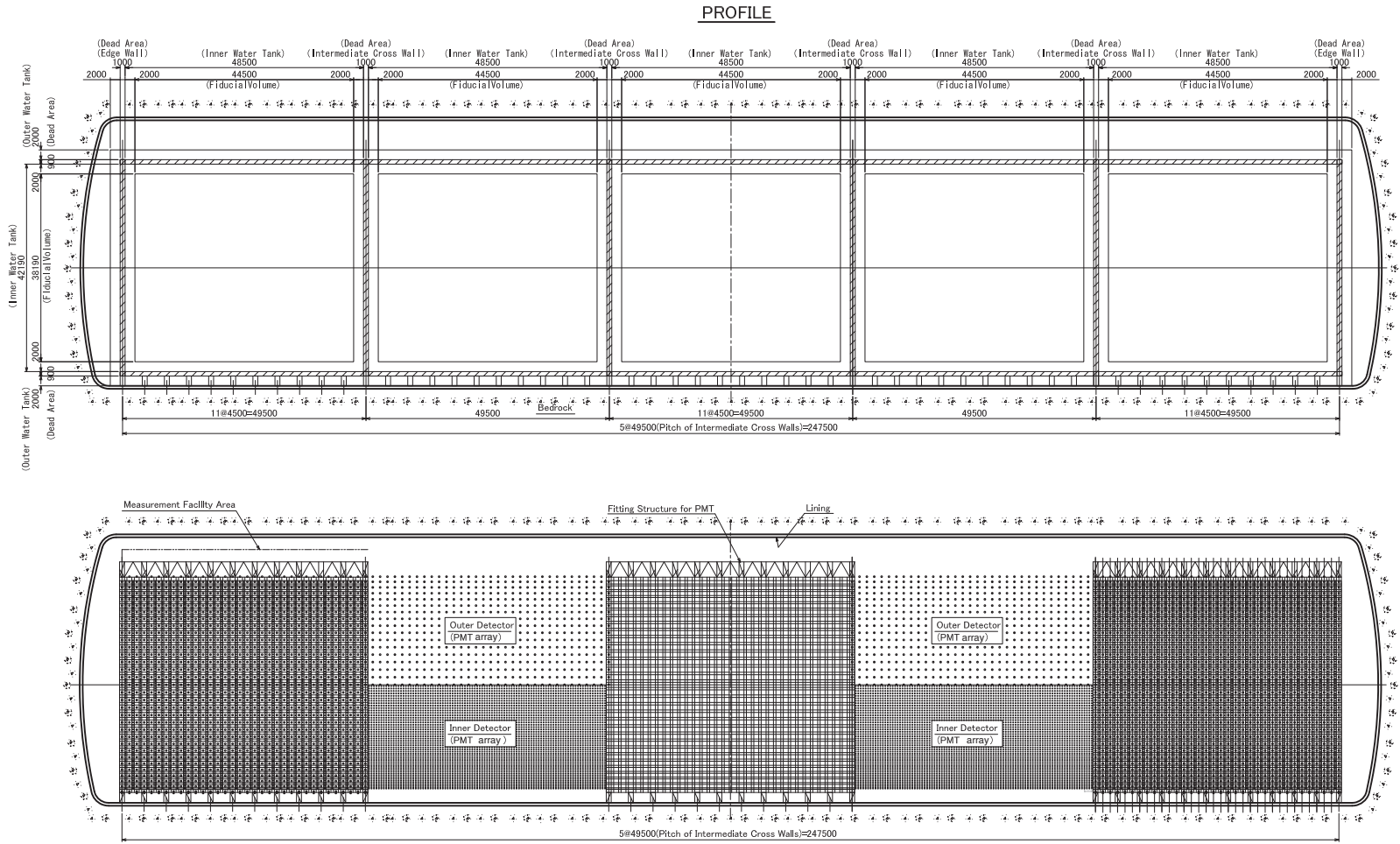
PROFILE

Fig. 4. Profile of the Hyper-K detector. Top: the detector segmentation. Bottom: PMT arrays and the support structure for the inner and outer detectors. Each quasi-cylindrical tank lying horizontally is segmented by intermediate walls into five compartments.
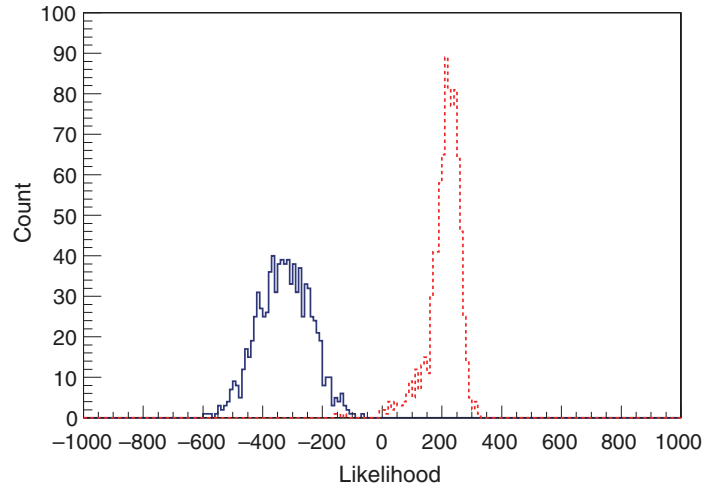
Fig. 5. PID likelihood functions for electrons (blue solid histogram) and μ (red dashed histogram) with 500 MeV/c momentum. A negative (positive) value indicates an electron-like (μ-like) particle.

Table 5. Comparison of the performance of SK-II (20% photo-coverage), SK-IV (40% photo-coverage), and the expected performance of the Hyper-Kamiokande baseline design (20% photo-coverage) with preliminary Hyper-K simulation and reconstruction.

	SK-II		SK-IV		Hyper-K	
Particle type ($p = 500$ MeV/c)	e	μ	e	μ	e	μ
Vertex resolution	28 cm	23 cm	25 cm	17 cm	27 cm	30 cm
Particle identification	98.5%	99.0%	98.8%	99.5%	>99.9%	99.2%
Momentum resolution	5.6%	3.6%	4.4%	2.3%	4.0%	2.6%

We have been careful to keep the possibility of gadolinium loading in mind when designing the overall Hyper-Kamiokande water system.

We have evaluated the expected performance of the Hyper-K detector using the MC simulation and reconstruction tools under development. We have been developing a detector simulation dedicated to Hyper-K based on "WCSim" [70], which is an open-source water Cherenkov detector simulator based on the GEANT4 library [71,72]. A new reconstruction algorithm developed for Super-K/T2K [11], named "fiTQun," has been adopted for the Hyper-K analysis. It uses a maximum likelihood fit with charge and time probability density functions constructed for every PMT hit assuming several sets of physics variables (such as vertex, direction, momentum, and particle type) [11,73].

As an example of the evaluation, electrons and muons with 500 MeV/c are generated with a fixed vertex (at the center of the tank) and direction (toward the barrel of the tank) in the Hyper-K detector simulation. Figure 5 shows the likelihood function for the particle identification. A negative (positive) value indicates an electron-like (μ-like) particle. It demonstrates a clear separation of electrons and muons. The obtained performance of Hyper-Kamiokande is compared with the performance of SK-II (20% photo coverage, old electronics) and SK-IV (40% photo coverage, new electronics) in Table 5. The vertex resolution for muon events will be improved to the same level as Super-K with an update of the reconstruction program. From the preliminary studies, the performance of Hyper-K is similar to or possibly better than SK-II or SK-IV with the new algorithm. In the physics sensitivity study described in Sect. 4, a Super-K full MC simulation with the SK-IV configuration is used

because it includes the simulation of new electronics and is tuned with real data, while giving a similar performance to Hyper-K, as demonstrated above.

4. Physics sensitivities

4.1. Overview

As discussed in Sect. 2.2, a comparison of muon-type to electron-type transition probabilities between neutrinos and anti-neutrinos is one of the most promising methods to observe the lepton CP asymmetry. Recent observation of a nonzero, rather large value of θ_{13} [10,14,41,42] makes this exciting possibility more realistic.

Figure 6 shows the $\nu_\mu \to \nu_e$ and $\bar{\nu}_\mu \to \bar{\nu}_e$ oscillation probabilities as a function of the true neutrino energy for a baseline of 295 km. The Earth matter density of 2.6 g/cm^3 is used in this analysis. The cases for $\delta_{CP} = 0, \frac{1}{2}\pi, \pi$, and $-\frac{1}{2}\pi$ are overlaid. Also shown are the cases of normal mass hierarchy ($\Delta m_{32}^2 > 0$) with solid lines and inverted mass hierarchy ($\Delta m_{32}^2 < 0$) with dashed lines. The oscillation probabilities depend on the value of δ_{CP}, and, by comparing the neutrinos and anti-neutrinos, one can see the effect of CP violation.

There are sets of different mass hierarchy and values of δ_{CP} that give similar oscillation probabilities. This is known as the degeneracy due to unknown mass hierarchy and may introduce an ambiguity if we do not know the true mass hierarchy. Because there are a number of experiments planned to determine mass hierarchy in the near future, it is expected that the mass hierarchy will be determined by the time Hyper-K starts to take data. If not, Hyper-K itself has a sensitivity to the mass hierarchy by the atmospheric neutrino measurements, as shown in Table 1. Furthermore, a combined analysis of the accelerator and atmospheric neutrino data in Hyper-K will enhance the sensitivity, as shown in Sect. 4.7. Thus, the mass hierarchy is assumed to be known in this analysis, unless otherwise stated.

Figure 7 shows the contribution from each term of the $\nu_\mu \to \nu_e$ oscillation probability formula, Eq. (7), for $L = 295$ km, $\sin^2 2\theta_{13} = 0.1$, $\sin^2 2\theta_{23} = 1.0$, $\delta_{CP} = \pi/2$, and normal mass hierarchy. For $E_\nu \simeq 0.6$ GeV, which gives $\sin \Delta_{32} \simeq \sin \Delta_{31} \simeq 1$,

$$\frac{P(\nu_\mu \to \nu_e) - P(\bar{\nu}_\mu \to \bar{\nu}_e)}{P(\nu_\mu \to \nu_e) + P(\bar{\nu}_\mu \to \bar{\nu}_e)} \simeq \frac{-16 J_{CP} \sin \Delta_{21} + 16 c_{13}^2 s_{13}^2 s_{23}^2 \frac{a}{\Delta m_{31}^2}\left(1 - 2s_{13}^2\right)}{8 c_{13}^2 s_{13}^2 s_{23}^2} \tag{10}$$

$$= -0.28 \sin \delta + 0.07. \tag{11}$$

The effect of the CP-violating term can be as large as 28%, while the matter effect is much smaller.

The uncertainty of Earth density between Tokai and Kamioka is estimated to be at most 6% [74]. Because the matter effect contribution to the total appearance probability is less than 10% for a 295 km baseline, the uncertainty from matter density is estimated to be less than 0.6% and is neglected in this analysis.

Due to the relatively short baseline and thus lower neutrino energy at the oscillation maximum, the contribution of the matter effect is smaller for the J-PARC to Hyper-Kamiokande experiment compared to other proposed experiments, like LBNE in the United States [75] or LBNO in Europe [76]. Thus the CP asymmetry measurement with the J-PARC to Hyper-K long-baseline experiment has less uncertainty related to the matter effect, while other experiments with >1000 km baseline have much better sensitivity to the mass hierarchy with accelerator neutrino beams[1]. The sensitivities for

---

[1] Note that Hyper-K has sensitivity to the mass hierarchy using atmospheric neutrinos, as shown in Table 1.
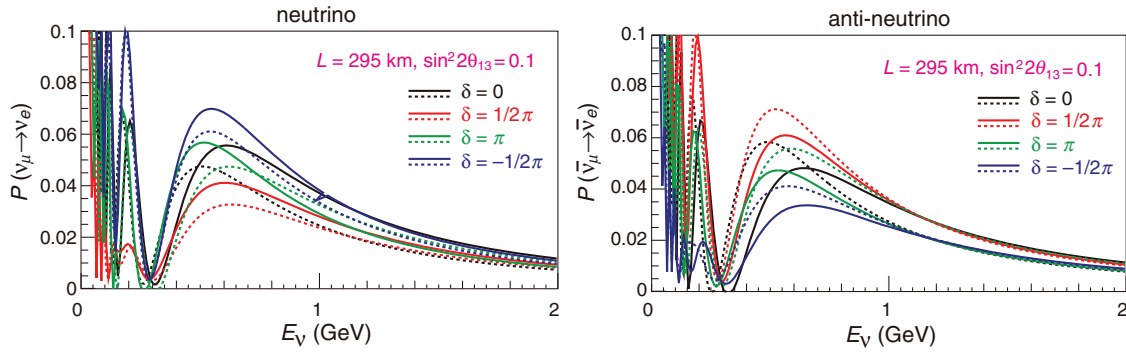
Fig. 6. Oscillation probabilities as a function of the neutrino energy for $\nu_\mu \to \nu_e$ (left) and $\bar{\nu}_\mu \to \bar{\nu}_e$ (right) transitions with $L = 295$ km and $\sin^2 2\theta_{13} = 0.1$. Black, red, green, and blue lines correspond to $\delta_{CP} = 0$, $\frac{1}{2}\pi$, π, and $-\frac{1}{2}\pi$, respectively. Solid (dashed) line represents the case for a normal (inverted) mass hierarchy.
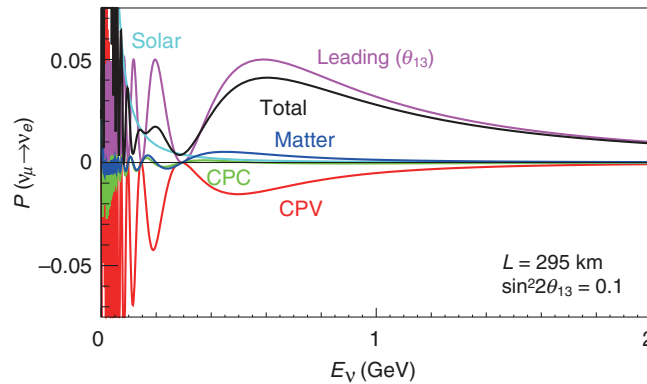
Fig. 7. Oscillation probability of $\nu_\mu \to \nu_e$ as a function of the neutrino energy with a baseline of 295 km. $\sin^2 2\theta_{13} = 0.1$, $\delta_{CP} = \frac{1}{2}\pi$, and normal hierarchy are assumed. The contribution from each term of the oscillation probability formula is shown separately.

CP violation and mass hierarchy can be further enhanced by combining measurements with different baselines.

The analysis method is based on a framework developed for the sensitivity study by T2K reported in Ref. [77]. A binned likelihood analysis based on the reconstructed neutrino energy distribution is performed using both ν_e ($\bar{\nu}_e$) appearance and ν_μ ($\bar{\nu}_\mu$) disappearance samples simultaneously. In addition to $\sin^2 2\theta_{13}$ and δ_{CP}, $\sin^2 \theta_{23}$ and Δm_{32}^2 are also included as free parameters in the fit. Table 6 shows the nominal oscillation parameters used in the study presented in this paper, and the treatment during the fitting. Systematic uncertainties are estimated based on the experience and prospects of the T2K experiment, and implemented as a covariance matrix that takes into account the correlation of uncertainties.

An integrated beam power of $7.5 \, \mathrm{MW} \times 10^7 \, \mathrm{s}$ is assumed in this study. It corresponds to 1.56×10^{22} protons on target with a 30 GeV J-PARC beam. We have studied the sensitivity to CP violation with various assumptions of neutrino mode and anti-neutrino mode beam running time ratio for both normal and inverted mass hierarchy cases. The dependence of the sensitivity on the $\nu : \bar{\nu}$ ratio is found to be not significant between $\nu : \bar{\nu} = 1:1$ to 1:5. In this paper, the $\nu : \bar{\nu}$ ratio is set to be 1:3 so that the expected number of events is approximately the same for the neutrino and anti-neutrino modes.

Table 6. Oscillation parameters used for the sensitivity analysis and treatment in the fitting. The *nominal* values are used for the figures and numbers in this section, unless otherwise stated.

Parameter	Nominal value	Treatment
$\sin^2 2\theta_{13}$	0.10	Fitted
δ_{CP}	0	Fitted
$\sin^2 \theta_{23}$	0.50	Fitted
Δm^2_{32}	$2.4 \times 10^{-3}\,\mathrm{eV}^2$	Fitted
Mass hierarchy	Normal or Inverted	Fixed
$\sin^2 2\theta_{12}$	0.8704	Fixed
Δm^2_{21}	$7.6 \times 10^{-5}\,\mathrm{eV}^2$	Fixed
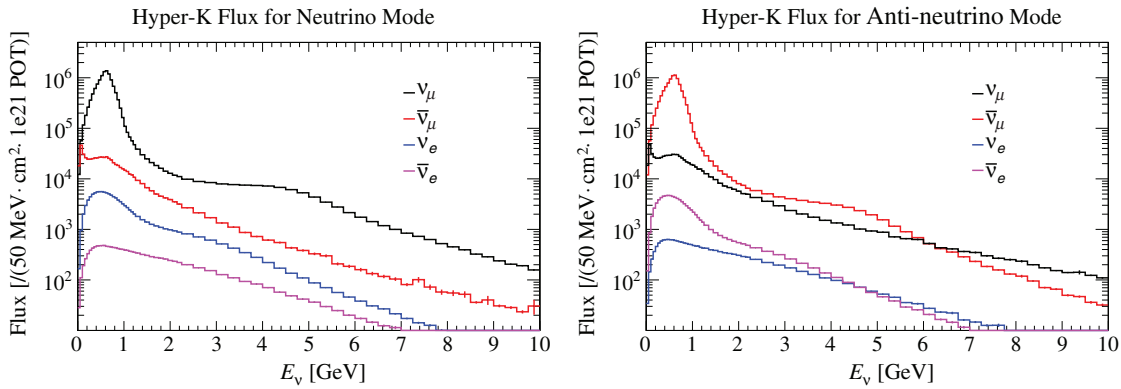
Fig. 8. The predicted Hyper-K neutrino fluxes from the J-PARC beam without oscillations. The neutrino enhanced beam is shown on the left and the anti-neutrino enhanced beam is shown on the right.

4.2.   Neutrino flux

The neutrino flux is estimated by the T2K Collaboration [78] by simulating the J-PARC neutrino beamline while tuning the modeling of hadronic interactions using data from NA61/SHINE [79, 80] and other experiments measuring hadronic interactions on nuclei. To date, NA61/SHINE has provided measurements of pion and kaon production multiplicities for proton interactions on a 0.04 interaction length graphite target, as well as the inelastic cross section for protons on carbon. Since "thin" target data are used, the secondary interactions of hadrons inside and outside the target are modeled using other data or scaling the NA61/SHINE data to different center-of-mass energies or target nuclei. NA61/SHINE also took data with a replica of the 90 cm-long T2K target, which will reduce the uncertainties related to the secondary interactions inside the target.

For the studies presented in this document, the T2K flux simulation has been used with the horn currents raised from 250 kA to 320 kA. The flux is estimated for both polarities of the horn fields, corresponding to neutrino enhanced and anti-neutrino enhanced fluxes. The calculated fluxes at Hyper-K, without oscillations, are shown in Fig. 8.

The sources of uncertainty in the T2K flux calculation include:

- Uncertainties on the primary production of pions and kaons in proton-on-carbon collisions.
- Uncertainties on the secondary hadronic interactions of particles in the target or beamline materials after the initial hadronic scatter.
- Uncertainties on the properties of the proton beam incident on the target, including the absolute current and the beam profile.
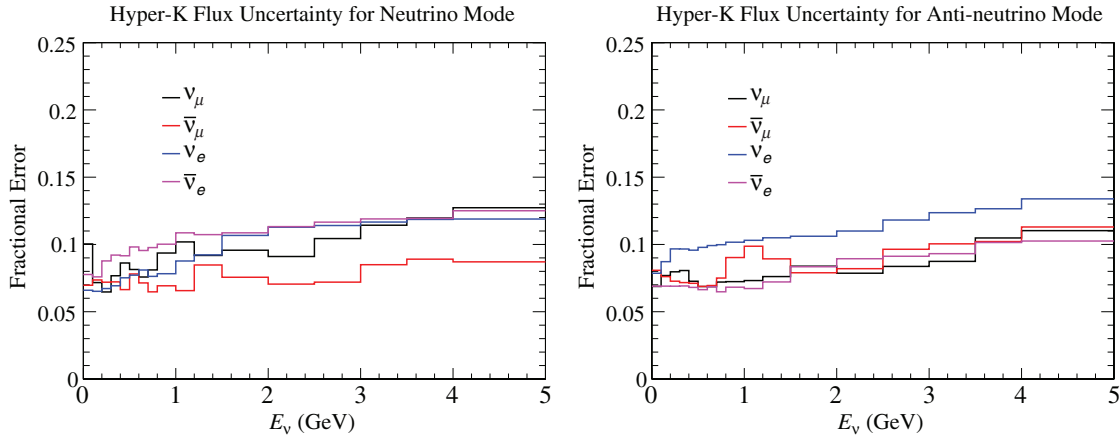
Fig. 9. The predicted uncertainty on the neutrino flux calculation assuming that replica target hadron production data are available.

- ○ Uncertainties on the alignment of beamline components, including the target and magnetic horns.
- ○ Uncertainties on the modeling of the horn fields, including the absolute field strength and asymmetries in the field.

The uncertainties on the hadronic interaction modeling are the largest contribution to the flux uncertainty and may be reduced by using the hadron production data with a replica of the T2K target. A preliminary analysis using a subset of the replica target data from NA61/SHINE has shown that it can be used to predict the T2K flux [81]. Since it is expected that replica target data will be available for future long-baseline neutrino experiments, the Hyper-K flux uncertainty is estimated assuming the expected uncertainties on the measurement of particle multiplicities from the replica target. Hence, uncertainties related to the modeling of hadronic interactions inside the target are no longer relevant; however, uncertainties for interactions outside the target are considered. The uncertainties on the measured replica target multiplicities are estimated by applying the same uncertainties that NA61/SHINE has reported for the thin target multiplicity measurements.

The total uncertainties on the flux as a function of the neutrino energy are shown in Fig. 9. In oscillation measurements, the predicted flux is used in combination with measurements of the neutrino interaction rate from near detectors. Hence, it is useful to consider the uncertainty on the ratio of the flux at the far and near detectors:

$$\delta_{\text{F/N}}(E_\nu) = \delta \left(\frac{\phi_{\text{HK}}(E_\nu)}{\phi_{\text{ND}}(E_\nu)} \right). \tag{12}$$

Here $\phi_{\text{HK}}(E_\nu)$ and $\phi_{\text{ND}}(E_\nu)$ are the predicted fluxes at Hyper-K and the near detector, respectively. T2K uses the ND280 off-axis detector located 280 m from the T2K target. At that distance, the beamline appears as a line source of neutrinos, compared to a point source seen by Hyper-K, and the far-to-near ratio is not flat. For near detectors placed further away, at, e.g., 1 or 2 km, the far-to-near flux ratio becomes flatter and there is better cancellation of the flux uncertainties between the near and far detectors. Figure 10 shows how the uncertainty on the far-to-near ratio evolves for baselines of 280 m, 1 km, and 2 km. While this extrapolation uncertainty is reduced for near detectors further from the production point, even the 280 m to Hyper-K uncertainty is less than 1% near the flux peak energy of 600 MeV.
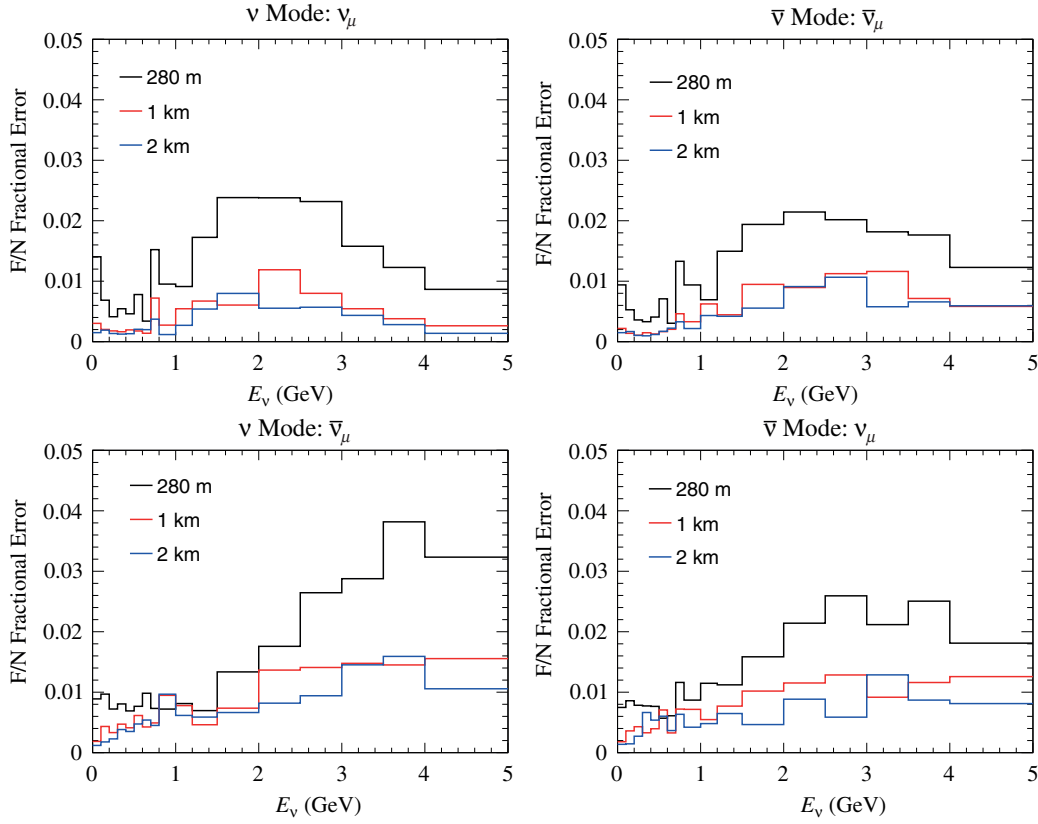
Fig. 10. The uncertainty on the far-to-near flux ratio for near detectors at 280 m, 1 km, and 2 km. Left: neutrino enhanced beam. Right: anti-neutrino enhanced beam. Top: the focused component of the beam. Bottom: the defocused component of the beam.

4.3.   Expected observables at Hyper-K

Interactions of neutrinos in the Hyper-K detector are simulated with the NEUT program library [82–84], which is used in both Super-K and T2K. The response of the detector is simulated using the Super-K full Monte Carlo simulation based on the GEANT3 package [85]. The simulation is based on the SK-IV configuration with upgraded electronics and DAQ system. Events are reconstructed with the Super-K reconstruction software. As described in Sect. 3.3, the performance of the Hyper-K detector for neutrinos with the J-PARC beam energy is expected to be similar to that of Super-K. Thus, the Super-K full simulation gives a realistic estimate of the Hyper-K performance.

The criteria for selecting ν_e and ν_μ candidate events are based on those developed for and established with the Super-K and T2K experiments. Fully contained (FC) events with a reconstructed vertex inside the fiducial volume (FV) and visible energy (E_{vis}) greater than 30 MeV are selected as FCFV neutrino event candidates. In order to enhance charged-current quasi-elastic (CCQE, $\nu_l + n \rightarrow l^- + p$ or $\bar{\nu}_l + p \rightarrow l^+ + n$) interaction, a single Cherenkov ring is required.

Assuming a CCQE interaction, the neutrino energy (E_ν^{rec}) is reconstructed from the energy of the final-state charged lepton (E_ℓ) and the angle between the neutrino beam and the charged lepton directions (θ_ℓ) as

$$E_\nu^{\mathrm{rec}} = \frac{2(m_n - V)E_\ell + m_p^2 - (m_n - V)^2 - m_\ell^2}{2(m_n - V - E_\ell + p_\ell \cos\theta_\ell)},$$ (13)
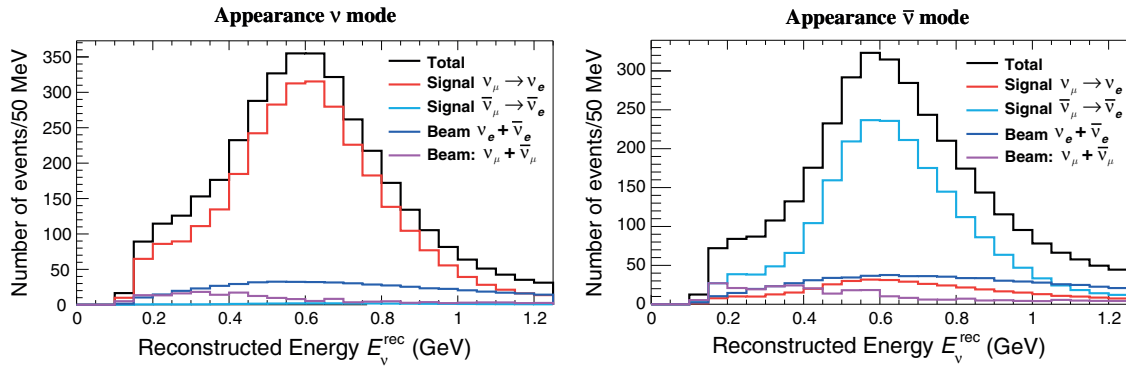
Fig. 11. Reconstructed neutrino energy distribution of the ν_e candidate events. Normal mass hierarchy with $\sin^2 2\theta_{13} = 0.1$ and $\delta_{CP} = 0$ are assumed.

Table 7. The expected number of ν_e candidate events. Normal mass hierarchy with $\sin^2 2\theta_{13} = 0.1$ and $\delta_{CP} = 0$ are assumed. Background (BG) is categorized by the flavor before oscillation.

	Signal		BG						
	$\nu_\mu \to \nu_e$	$\overline{\nu}_\mu \to \overline{\nu}_e$	ν_μ CC	$\overline{\nu}_\mu$ CC	ν_e CC	$\overline{\nu}_e$ CC	NC	BG total	Total
ν mode	3016	28	11	0	503	20	172	706	3750
$\overline{\nu}$ mode	396	2110	4	5	222	396	265	891	3397

where m_n, m_p, m_ℓ are the masses of the neutron, proton, and charged lepton, respectively, p_ℓ is the charged lepton momentum, and V is the nuclear potential energy (27 MeV).

Then, to select $\nu_e/\overline{\nu}_e$ candidate events, the following criteria are applied:

○ The reconstructed ring is identified as electron-like (e-like).
○ The visible energy (E_{vis}) is greater than 100 MeV.
○ There is no decay electron associated to the event.
○ The reconstructed energy (E_ν^{rec}) is less than 1.25 GeV.
○ In order to reduce the background from mis-reconstructed π^0 events, additional criteria using a reconstruction algorithm recently developed for T2K (fiTQun; see Sect. 3.3) is applied. With a selection based on the reconstructed π^0 mass and the ratio of the best-fit likelihoods of the π^0 and electron fits as used in T2K [11], the remaining π^0 background is reduced to about 30% compared to the previous study [15].

Figure 11 shows the reconstructed neutrino energy distributions of ν_e events after all the selections. The expected number of ν_e candidate events is shown in Table 7 for each signal and background component. In the neutrino mode, the dominant background component is intrinsic ν_e contamination in the beam. The mis-identified neutral-current π^0 production events are suppressed thanks to the improved π^0 rejection. In the anti-neutrino mode, in addition to $\overline{\nu}_e$ and $\overline{\nu}_\mu$, the ν_e and ν_μ components have non-negligible contributions due to larger fluxes and cross sections compared to their counterparts in the neutrino mode.

For the $\nu_\mu/\overline{\nu}_\mu$ candidate events, the following criteria are applied:

○ The reconstructed ring is identified as muon-like (μ-like).
○ The reconstructed muon momentum is greater than 200 MeV/c.
○ There is at most one decay electron associated to the event.
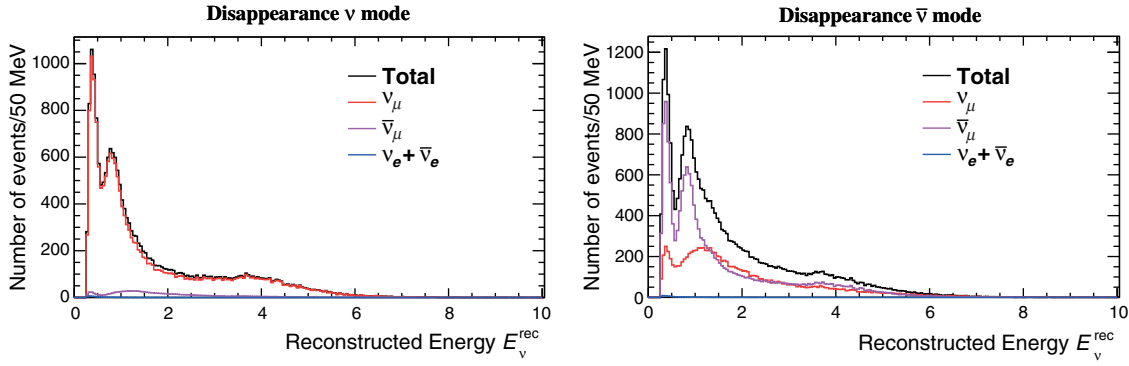
Fig. 12. Reconstructed neutrino energy distribution of the ν_μ candidate events.

Table 8. The expected number of ν_μ candidate events.

	ν_μ CC	$\overline{\nu}_\mu$ CC	ν_e CC	$\overline{\nu}_e$ CC	NC	$\nu_\mu \rightarrow \nu_e$	Total
ν mode	17 225	1088	11	1	999	49	19 372
$\overline{\nu}$ mode	10 066	15 597	7	7	1281	6	26 964

Figure 12 shows the reconstructed neutrino energy distributions of the selected $\nu_\mu/\overline{\nu}_\mu$ events. Table 8 shows the number of ν_μ candidate events for each signal and background component. For the neutrino mode, most of the events are due to ν_μ, while in the anti-neutrino mode the contribution from wrong-sign ν_μ components is significant.

The reconstructed neutrino energy distributions of ν_e events for several values of δ_{CP} are shown in the top plots of Fig. 13. The effect of δ_{CP} is clearly seen using the reconstructed neutrino energy. The bottom plots show the differences in reconstructed energy spectra from $\delta_{CP} = 0°$ for the cases $\delta = 90°, -90°$, and $180°$. The error bars correspond to the statistical uncertainty. By using not only the total number of events but also the reconstructed energy distribution, the sensitivity to δ_{CP} can be improved, and one can discriminate all the values of δ_{CP}, including the difference between $\delta_{CP} = 0$ and π. Figure 14 shows the reconstructed neutrino energy distributions of the ν_μ sample for several values of δ_{CP}. As expected, the difference is very small for ν_μ events.

4.4. Analysis method

The sensitivity of a long-baseline experiment using Hyper-K and the J-PARC neutrino beam is studied using a binned likelihood analysis based on the reconstructed neutrino energy distribution. Both ν_e appearance and ν_μ disappearance samples, in both neutrino and anti-neutrino runs, are simultaneously fitted.
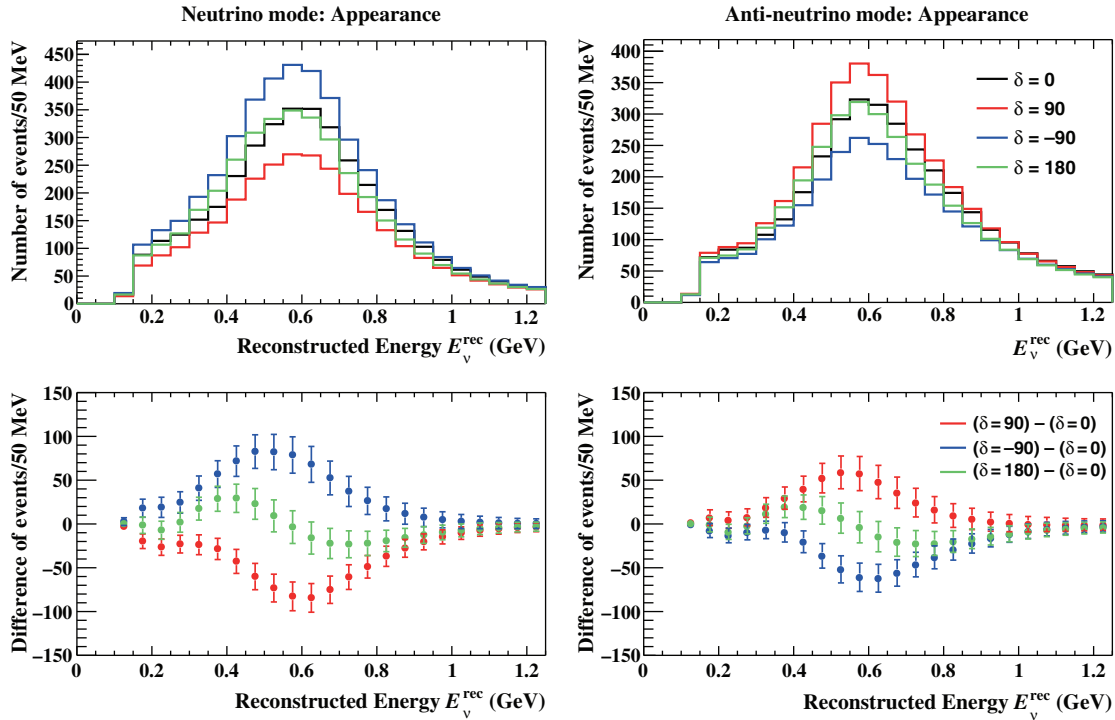
The χ^2 used in this study is defined as

$$\chi^2 = -2 \ln \mathcal{L} + P, \tag{14}$$

where $\ln \mathcal{L}$ is the log likelihood of a Poisson distribution,

$$-2 \ln \mathcal{L} = \sum_k \left\{ -N_k^{\text{test}}(1 + f_i) + N_k^{\text{true}} \ln \left[N_k^{\text{test}}(1 + f_i) \right] \right\}. \tag{15}$$

Here, $N_k^{\text{true}} \left(N_k^{\text{test}} \right)$ is the number of events in the kth reconstructed energy bin for the true (test) oscillation parameters. The index k runs over all reconstructed energy bins for muon and electron neutrino

Fig. 13. Top: Reconstructed neutrino energy distribution for several values of δ_{CP}. $\sin^2 2\theta_{13} = 0.1$ and normal hierarchy is assumed. Bottom: Differences in the reconstructed neutrino energy distributions from the case with $\delta_{CP} = 0°$. The error bars represent the statistical uncertainties of each bin.
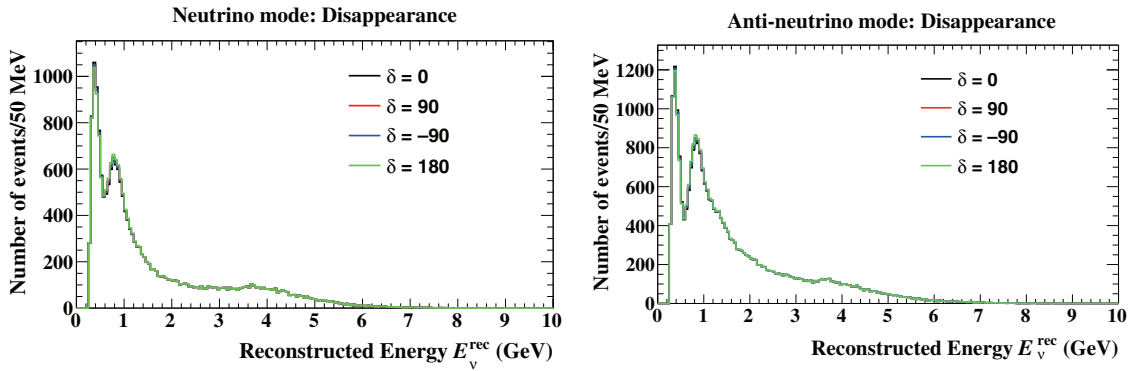
Fig. 14. Reconstructed neutrino energy distribution of ν_μ candidates for several values of δ_{CP}.

samples and for neutrino and anti-neutrino mode running. The parameters f_i represent systematic uncertainties. For anti-neutrino mode samples, an additional overall normalization parameter with 6% prior uncertainty is introduced to account for a possible uncertainty in the anti-neutrino interaction, which is less known experimentally in this energy region. This additional uncertainty is expected to decrease as we accumulate and analyze more anti-neutrino data in T2K, but we conservatively assign the current estimate for this study. A normalization weight $\left(1 + f_{\text{norm}}^{\bar{\nu}}\right)$ is multiplied to N_k^{test} in the anti-neutrino mode samples.

The penalty term P in Eq. (14) constrains the systematic parameters f_i with the normalized covariance matrix C:

$$P = \sum_{i,j} f_i \left(C^{-1}\right)_{i,j} f_j. \tag{16}$$

In order to reduce the number of the systematic parameters, several reconstructed energy bins that have similar covariance values are merged for f_i.

The size of the systematic uncertainty is evaluated based on the experience and prospects of the T2K experiment, as it provides the most realistic estimate as the baseline. We estimate the systematic uncertainties assuming the T2K neutrino beamline and near detectors, taking into account improvements expected with future T2K running and analysis improvements. For Hyper-K, a further reduction of systematic uncertainties will be possible with upgrade of the beamline and near detectors, improvements in detector calibration and analysis techniques, and improved understanding of neutrino interaction with more measurements. In particular, as described in Sect. 3.2, studies of near detectors are ongoing with a goal of further reducing systematic uncertainties. The sensitivity update is expected in the near future as the near-detector design studies advance.

There are three main categories of systematic uncertainties. We assume improvement from the current T2K uncertainties for each category as follows.

i) Flux and cross-section uncertainties constrained by the fit to current near-detector data: These arise from systematics of the near detectors. The understanding of the detector will improve in the future, but this category of uncertainties is conservatively assumed to stay at the same level as currently estimated.

ii) Cross-section uncertainties that are not constrained by the fit to current near-detector data: Errors in this category will be reduced as more categories of samples are added to the near-detector data fit, which constrains the cross-section models. We assume that the uncertainties arising from different target nuclei between the near and far detectors will become negligible by including the measurement with the water target in the near detector.

iii) Uncertainties on the far-detector efficiency and reconstruction modeling: Because most of them are estimated by using atmospheric neutrinos as a control sample, errors in this category are expected to decrease with the statistics available with Hyper-K, which is more than an order of magnitude larger than that currently used for T2K. Uncertainties arising from the energy scale are kept the same because they are not estimated by the atmospheric neutrino sample.

The flux and cross-section uncertainties are assumed to be uncorrelated between the neutrino and anti-neutrino running, except for the uncertainty in the ν_e/ν_μ cross-section ratio, which is treated as anti-correlated considering the theoretical uncertainties studied in Ref. [86]. Because some of the uncertainties, such as those from the cross-section modeling or near-detector systematics, are expected to be correlated and give more of a constraint, this is a conservative assumption. The far-detector uncertainty is treated as fully correlated between the neutrino and anti-neutrino running.

Figures 15 and 16 show the fractional systematic uncertainties for the appearance and disappearance reconstructed energy spectra in neutrino and anti-neutrino mode, respectively. Black lines represent the prior uncertainties and bin widths of the systematic parameters f_i, while colored lines show the contribution from each uncertainty source. Figure 17 shows the correlation matrix of the systematic uncertainties between the reconstructed neutrino energy bins of the four samples. The systematic uncertainties (in %) of the number of expected events at the far detector are summarized in Table 9.

4.5.   Expected sensitivity to CP violation

Figure 18 shows the 90% CL allowed regions on the $\sin^2 2\theta_{13}$–δ_{CP} plane. The results for the true values of $\delta_{CP} = (-90°, 0, 90°, 180°)$ are overlaid. The top (bottom) plot shows the case for the normal
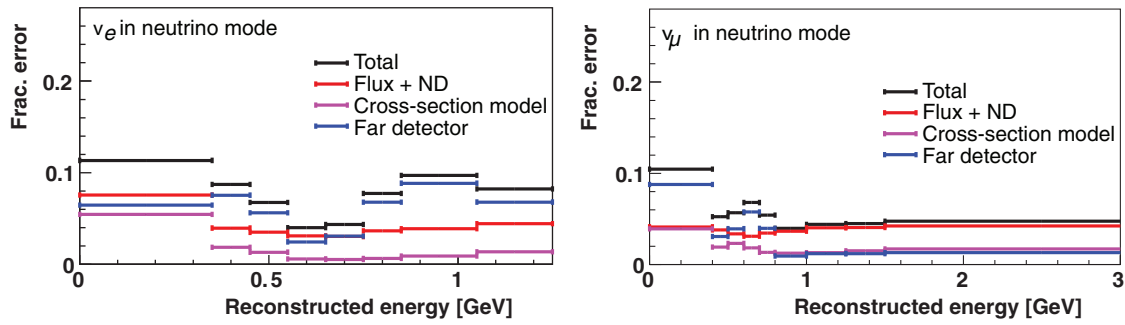
Fig. 15. Fractional error size for the appearance (left) and disappearance (right) samples in the neutrino mode. Black: total uncertainty, red: flux and cross section constrained by the near detector, magenta: near-detector non-constrained cross section, blue: far-detector error.
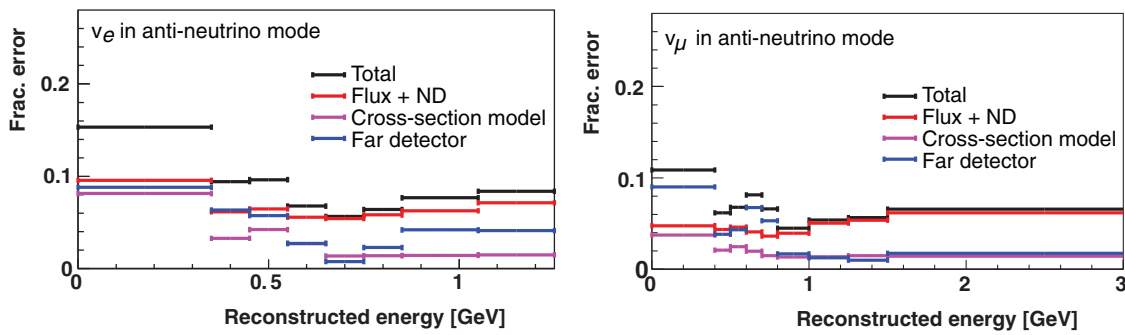

Fig. 16. Fractional error size for the appearance (left) and disappearance (right) samples in the anti-neutrino mode. Black: total uncertainty, red: flux and cross section constrained by the near detector, magenta: near-detector non-constrained cross section, blue: far-detector error.
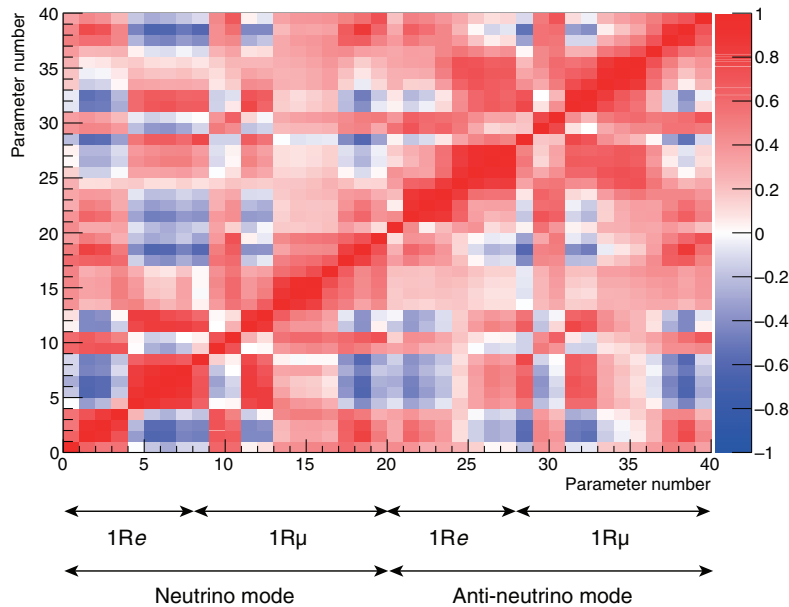
Fig. 17. Correlation matrix between reconstructed energy bins of the four samples due to the systematic uncertainties. Bins 1–8, 9–20, 21–28, and 29–40 correspond to the neutrino-mode single-ring e-like, the neutrino-mode single-ring μ-like, the anti-neutrino-mode single-ring e-like, and the anti-neutrino-mode single-ring μ-like samples, respectively.

Table 9. Uncertainties (in %) for the expected number of events at Hyper-K from the systematic uncertainties assumed in this study. ND: near detector.

		Flux & ND-constrained cross section	ND-independent cross section	Far detector	Total
ν mode	Appearance	3.0	1.2	0.7	3.3
	Disappearance	2.8	1.5	1.0	3.3
$\bar{\nu}$ mode	Appearance	5.6	2.0	1.7	6.2
	Disappearance	4.2	1.4	1.1	4.5
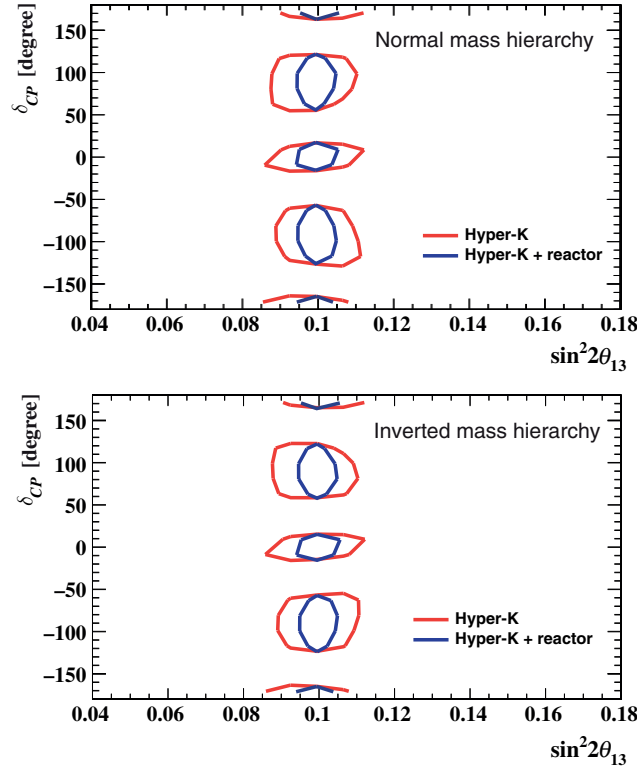
Fig. 18. The 90% CL allowed regions in the $\sin^2 2\theta_{13}$–δ_{CP} plane. The results for the true values of $\delta_{CP} = (-90°, 0, 90°, 180°)$ are overlaid. Top: normal hierarchy case. Bottom: inverted hierarchy case. Red (blue) lines show the result with Hyper-K only (with a $\sin^2 2\theta_{13}$ constraint from reactor experiments).

(inverted) mass hierarchy. Also shown are the allowed regions when we include a constraint from the reactor experiments, $\sin^2 2\theta_{13} = 0.100 \pm 0.005$. With reactor constraints, although the contour becomes narrower in the direction of $\sin^2 2\theta_{13}$, the sensitivity to δ_{CP} does not significantly change because δ_{CP} is constrained by the comparison of neutrino and anti-neutrino oscillation probabilities by Hyper-K and not limited by the uncertainty of θ_{13}.

Figure 19 shows the expected significance to exclude $\sin \delta_{CP} = 0$ (the CP conserved case). The significance is calculated as $\sqrt{\Delta \chi^2}$, where $\Delta \chi^2$ is the difference in χ^2 for the *trial* value of δ_{CP} and for $\delta_{CP} = 0°$ or $180°$ (the smaller value of difference is taken). We have also studied the case with a reactor constraint, but the result changes only slightly. Figure 20 shows the fraction of δ_{CP} for which $\sin \delta_{CP} = 0$ is excluded with more than 3σ and 5σ significance as a function of the integrated beam power. The ratio of integrated beam power for the neutrino and anti-neutrino modes is fixed to 1:3. Normal mass hierarchy is assumed. The results for the inverted hierarchy are almost the same.
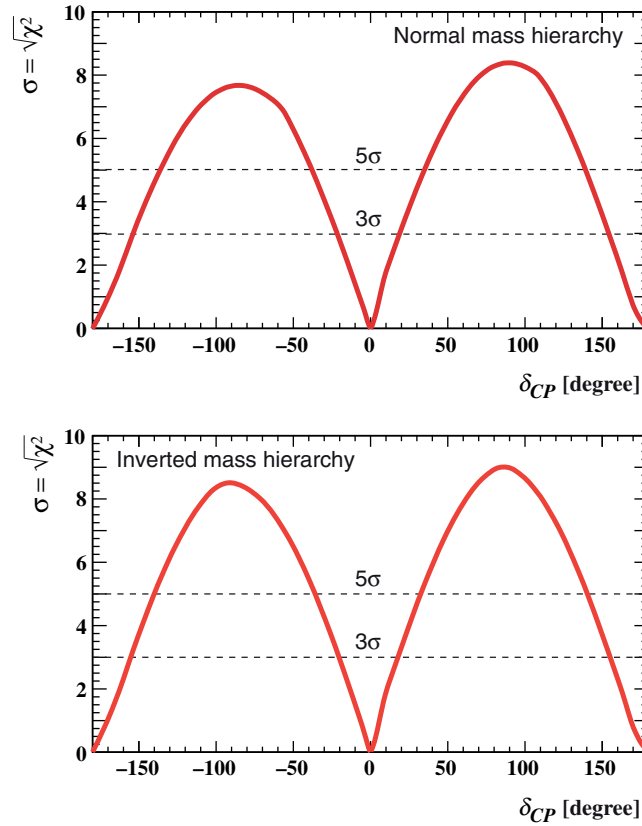
Fig. 19. Expected significance to exclude $\sin \delta_{CP} = 0$. Top: normal hierarchy case. Bottom: inverted hierarchy case.
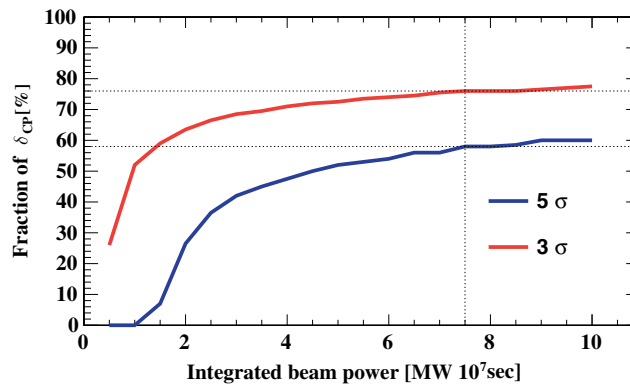
Fig. 20. Fraction of δ_{CP} for which $\sin \delta_{CP} = 0$ can be excluded with more than 3σ (red) and 5σ (blue) significance as a function of the integrated beam power for the normal hierarchy case. The ratio of the neutrino and anti-neutrino modes is fixed to 1:3.

CP violation in the lepton sector can be observed with more than $3(5)\sigma$ significance for 76(58)% of the possible values of δ_{CP}.

Figure 21 shows the 68% CL uncertainty of δ_{CP} as a function of the integrated beam power. With $7.5 \, \mathrm{MW} \times 10^7$ s of exposure (1.56×10^{22} protons on target), the value of δ_{CP} can be determined to better than $19°$ for all values of δ_{CP}.
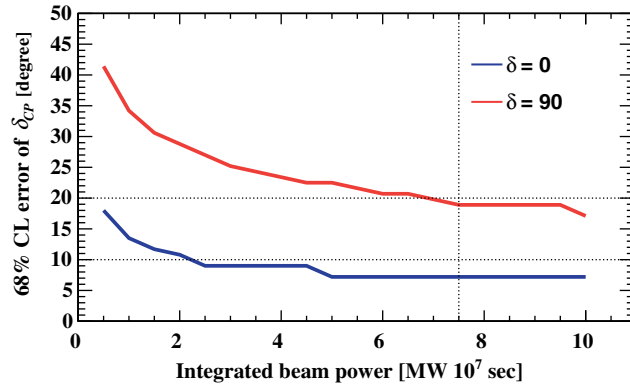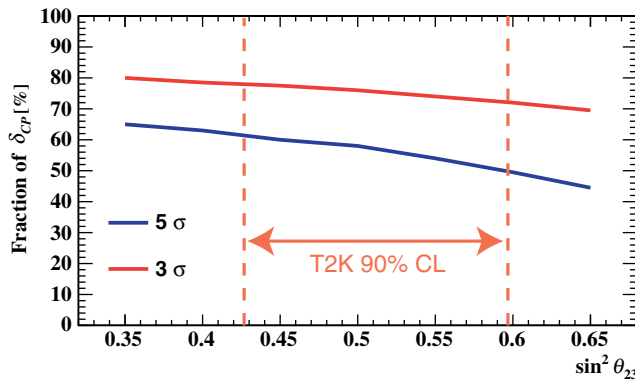
Fig. 21. Expected 68% CL uncertainty of δ_{CP} as a function of integrated beam power.

Fig. 22. Fraction of δ_{CP} for which $\sin \delta_{CP} = 0$ can be excluded with more than 3σ (red) and 5σ (blue) significance as a function of the true value of $\sin^2 \theta_{23}$, for the normal hierarchy case. Vertical dashed lines indicate 90% confidence intervals of $\sin^2 \theta_{23}$ from the T2K measurement in 2014 [38].
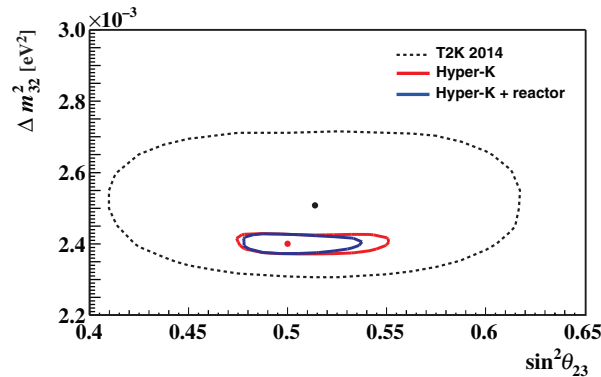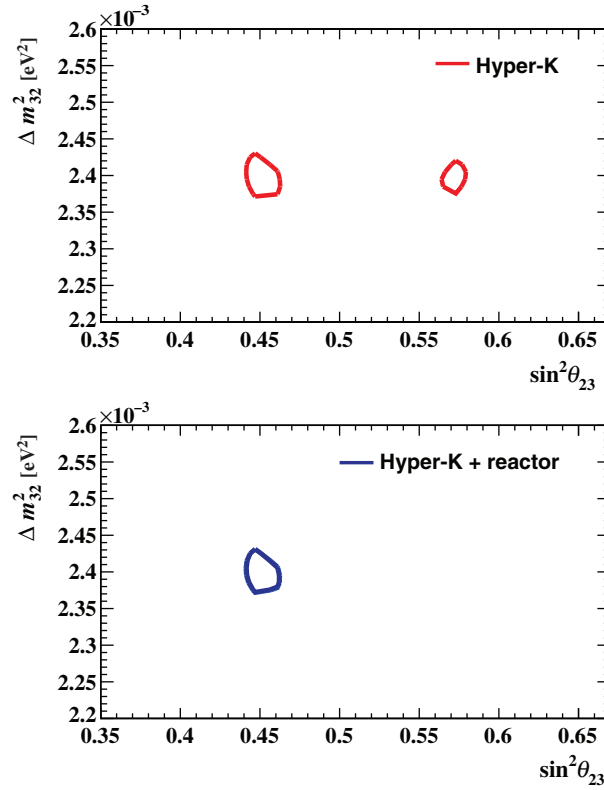
Fig. 23. The 90% CL allowed regions in the $\sin^2 \theta_{23}$–Δm^2_{32} plane. The true values are $\sin^2 \theta_{23} = 0.5$ and $\Delta m^2_{32} = 2.4 \times 10^{-3} \, \text{eV}^2$ (red point). The effect of systematic uncertainties is included. The red (blue) line corresponds to the result with Hyper-K alone (with a reactor constraint on $\sin^2 2\theta_{13}$). The dotted line is the 90% CL contour from the T2K experiment [38] with the best-fit values indicated by a black point.

As a nominal value, we use $\sin^2 \theta_{23} = 0.5$, but the sensitivity to CP violation depends on the value of θ_{23}. Figure 22 shows the fraction of δ_{CP} for which $\sin \delta_{CP} = 0$ is excluded with more than 3σ and 5σ significance as a function of the true value of $\sin^2 \theta_{23}$ with the current best knowledge of the possible $\sin^2 \theta_{23}$ range from the T2K Collaboration [38].

Fig. 24. 90% CL allowed regions in the $\sin^2\theta_{23}$–Δm^2_{32} plane. The true values are $\sin^2\theta_{23} = 0.45$ and $\Delta m^2_{32} = 2.4 \times 10^{-3}$ eV^2. The effect of systematic uncertainties is included. Top: Hyper-K only. Bottom: With a reactor constraint.

Table 10. Expected 1σ uncertainty of Δm^2_{32} and $\sin^2\theta_{23}$ for true $\sin^2\theta_{23} = 0.45, 0.50, 0.55$. A reactor constraint on $\sin^2 2\theta_{13} = 0.1 \pm 0.005$ is imposed. NH: normal hierarchy, IH: inverted hierarchy.

True $\sin^2\theta_{23}$	0.45		0.50		0.55	
Parameter	Δm^2_{32} (eV^2)	$\sin^2\theta_{23}$	Δm^2_{32} (eV^2)	$\sin^2\theta_{23}$	Δm^2_{32} (eV^2)	$\sin^2\theta_{23}$
NH	1.4×10^{-5}	0.006	1.4×10^{-5}	0.015	1.5×10^{-5}	0.009
IH	1.5×10^{-5}	0.006	1.4×10^{-5}	0.015	1.5×10^{-5}	0.009

4.6. Sensitivity to Δm^2_{32} and $\sin^2\theta_{23}$

The result shown above is obtained with $\sin^2\theta_{23}$ and Δm^2_{32} as free parameters as well as $\sin^2 2\theta_{13}$ and δ_{CP}, with nominal parameters shown in Table 6. The use of the ν_μ sample in addition to ν_e enables us to also precisely measure $\sin^2\theta_{23}$ and Δm^2_{32}. Figure 23 shows the 90% CL allowed regions for the true value of $\sin^2\theta_{23} = 0.5$ together with the 90% CL contour by the T2K ν_μ disappearance measurement [38]. Hyper-K will be able to provide a precise measurement of $\sin^2\theta_{23}$ and Δm^2_{32}. Figure 24 shows the 90% CL allowed regions on the $\sin^2\theta_{23}$–Δm^2_{32} plane, for the true values of $\sin^2\theta_{23} = 0.45$ and $\Delta m^2_{32} = 2.4 \times 10^{-3}$ eV^2. For the determination of θ_{23}, a ν_μ disappearance measurement provides a precise measurement of $\sin^2 2\theta_{23}$. However, when $\theta_{23} \neq \frac{\pi}{4}$, there are two possible solutions (θ_{23} and $\frac{\pi}{2} - \theta_{23}$), which give the same $\sin^2 2\theta_{23}$. This is known as the octant degeneracy. As seen from Eq. (7), the ν_e appearance measurement can determine $\sin^2\theta_{23} \sin^2 2\theta_{13}$. In addition, the reactor experiments provide an almost pure measurement of $\sin^2 2\theta_{13}$. Thus, the
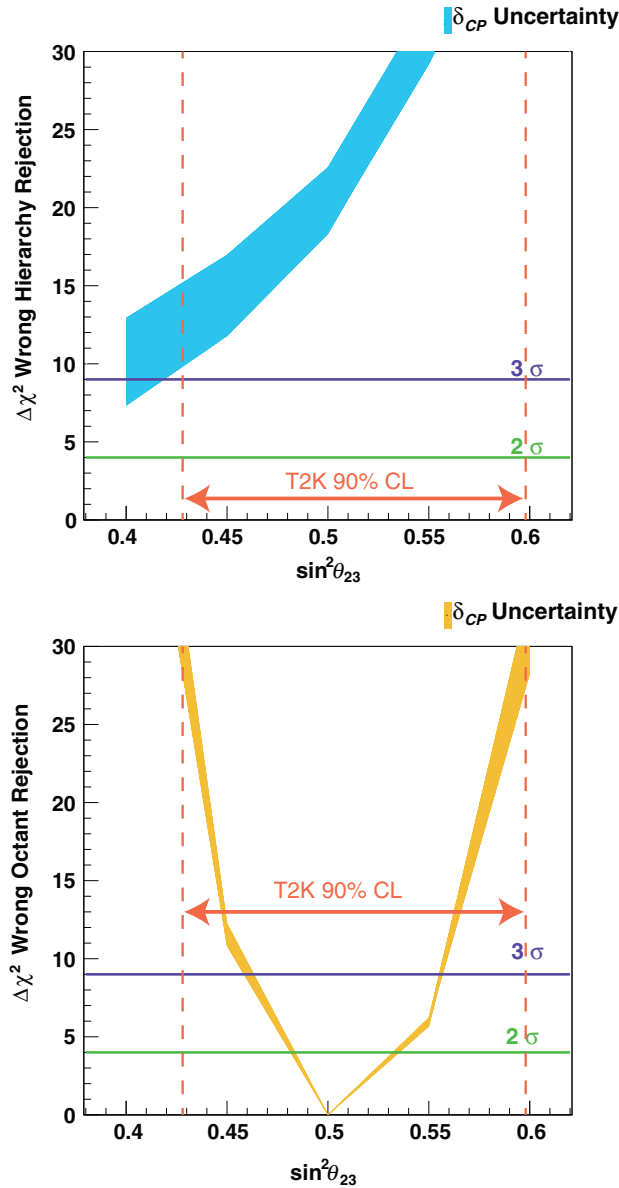
Fig. 25. Atmospheric neutrino sensitivities for a 10 yr exposure of Hyper-K assuming that the mass hierarchy is normal. Top: the $\Delta\chi^2$ discrimination of the wrong hierarchy hypothesis as a function of the assumed true value of $\sin^2\theta_{23}$. Bottom: the discrimination between the wrong octant for each value of $\sin^2\theta_{23}$. The uncertainty from δ_{CP} is represented by the thickness of the band. Vertical dashed lines indicate 90% confidence intervals of $\sin^2\theta_{23}$ from the T2K measurement in 2014 [38].

combination of these complementary measurements is known to be able to resolve this degeneracy if θ_{23} is sufficiently away from $\frac{\pi}{4}$ [87–89]. As shown in Fig. 24, with a constraint on $\sin^2 2\theta_{13}$ from the reactor experiments, Hyper-K measurements can resolve the octant degeneracy and precisely determine $\sin^2\theta_{23}$.

The expected precision of Δm^2_{32} and $\sin^2\theta_{23}$ for true $\sin^2\theta_{23} = 0.45, 0.50, 0.55$ with a reactor constraint on $\sin^2 2\theta_{13}$ is summarized in Table 10.

4.7.   Combination with atmospheric neutrino data

Atmospheric neutrinos can provide independent and complementary information to the accelerator beam program on the study of neutrino oscillation. For example, through the matter effect inside the
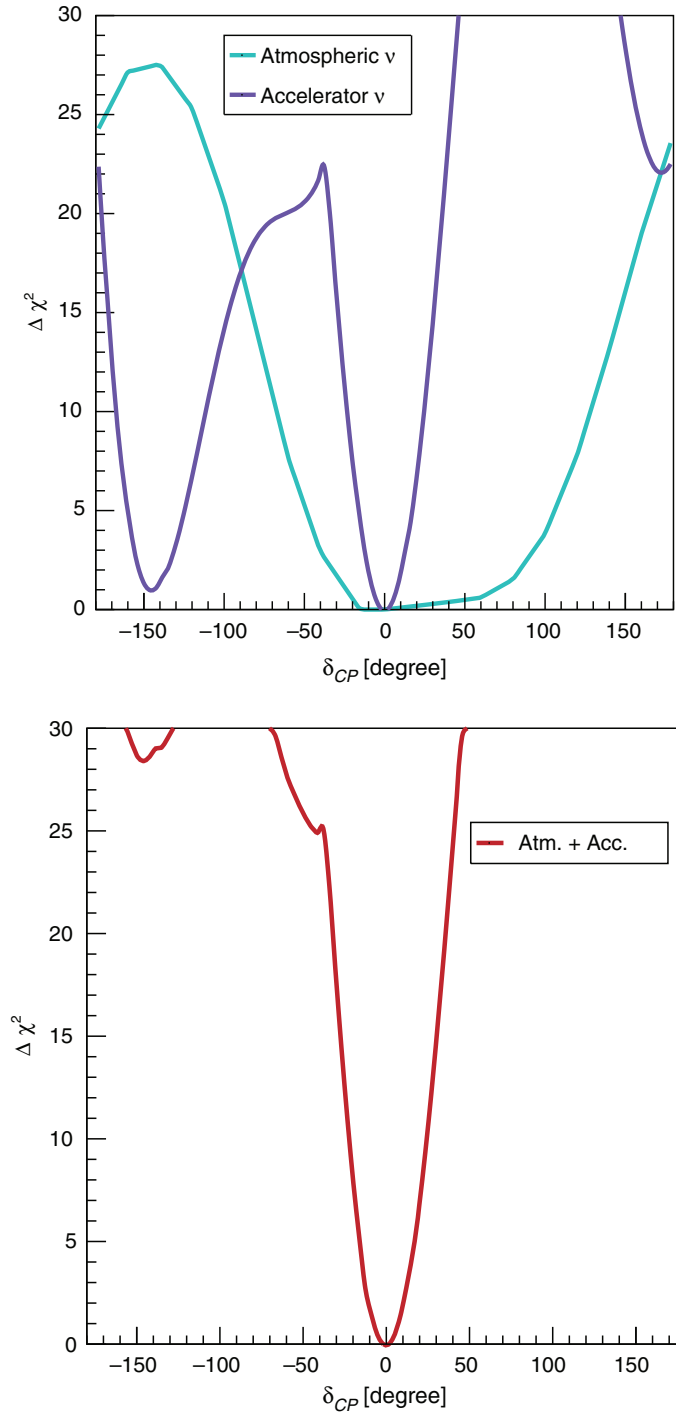
Fig. 26. Combination of the accelerator and atmospheric data. Top: Expected $\Delta\chi^2$ values for accelerator and atmospheric neutrino measurements assuming that the mass hierarchy is unknown. The true mass hierarchy is normal hierarchy and the true value of $\delta_{CP} = 0$. Bottom: By combining the two measurements, the sensitivity can be enhanced. In this example study, $\Delta\chi^2$ is simply added.

Earth, a large-statistics sample of atmospheric neutrinos by Hyper-K will have a good sensitivity to the mass hierarchy and θ_{23} octant.

Assuming a 10 yr exposure, Hyper-K's sensitivity to the mass hierarchy and the octant of θ_{23} by atmospheric neutrino data are shown in Fig. 25. Depending on the true value of θ_{23}, the sensitivity

changes considerably, but for all currently allowed values of this parameter the mass hierarchy sensitivity exceeds 3σ independent of the assumed hierarchy. If θ_{23} is non-maximal, the atmospheric neutrino data can be used to discriminate the octant at 3σ if $\sin^2\theta_{23} < 0.46$ or $\sin^2\theta_{23} > 0.56$.

In the previous sections, the mass hierarchy is assumed to be known prior to the Hyper-K measurements. This is a reasonable assumption considering the increased opportunities, thanks to a large value of θ_{13}, of ongoing and proposed projects for mass hierarchy determination. However, even if the mass hierarchy is unknown before the start of experiment, Hyper-K itself will be able to determine it with the atmospheric neutrino measurements.

Because Hyper-K will observe both accelerator and atmospheric neutrinos with the same detector, the physics capability of the project can be enhanced by combining two complementary measurements. As a demonstration of such a capability, a study has been done by simply adding $\Delta\chi^2$ from two measurements, although in a real experiment a more sophisticated analysis is expected. Assuming the true mass hierarchy of normal hierarchy and the true value of $\delta_{CP} = 0$, the values of expected $\Delta\chi^2$ as a function of δ_{CP} for each of the accelerator and atmospheric neutrino measurements, *without* assumption of prior mass hierarchy knowledge, are shown in the top plot of Fig. 26. For the accelerator neutrino measurement, there is a second minimum near $\delta_{CP} = 150°$ because of a degeneracy with mass hierarchy assumptions. On the other hand, the atmospheric neutrino measurement can discriminate the mass hierarchy, but the sensitivity to the CP-violating phase δ_{CP} is worse than the accelerator measurement. By adding the information from both measurements, as shown in the bottom plot of Fig. 26, the fake solution can be eliminated and a precise measurement of δ_{CP} will be possible.

5.   Conclusion

The sensitivity to leptonic CP asymmetry of a long-baseline experiment using a neutrino beam directed from J-PARC to the Hyper-Kamiokande detector has been studied based on a full simulation of beamline and detector. With an integrated beam power of $7.5\,\mathrm{MW} \times 10^7$ s, the value of δ_{CP} can be determined to better than $19°$ for all values of δ_{CP}, and CP violation in the lepton sector can be observed with more than 3σ (5σ) significance for 76% (58%) of the possible values of δ_{CP}.

Using both ν_e appearance and ν_μ disappearance data, a precise measurement of $\sin^2\theta_{23}$ will be possible. The expected 1σ uncertainty is 0.015(0.006) for $\sin^2\theta_{23} = 0.5(0.45)$.

References

[1] Y. Fukuda et al., Phys. Rev. Lett. **81**, 1562 (1998).
[2] P. Minkowski, Phys. Lett. B **67**, 421 (1977).
[3] M. Gell-Mann, P. Ramond, and R. Slansky, Conf. Proc. **C790927**, 315 (1979).
[4] T. Yanagida, Conf. Proc. **C7902131**, 95 (1979).

[5] R. N. Mohapatra and G. Senjanovic, Phys. Rev. Lett. **44**, 912 (1980).
[6] M. Fukugita and T. Yanagida, Phys. Lett. B **174**, 45 (1986).
[7] M. Kobayashi and T. Maskawa, Prog. Theor. Phys. **49**, 652 (1973).
[8] S. Fukuda et al., Phys. Rev. Lett. **86**, 5656 (2001).
[9] Q. R. Ahmad et al., Phys. Rev. Lett. **87**, 071301 (2001).
[10] K. Abe et al., Phys. Rev. Lett. **107**, 041801 (2011).
[11] K. Abe et al., Phys. Rev. Lett. **112**, 061802 (2014).
[12] F. P. An et al., Phys. Rev. Lett. **112**, 061801 (2014).
[13] Y. Abe et al., Phys. Lett. B **735**, 51 (2014).
[14] J. K. Ahn et al., Phys. Rev. Lett. **108**, 191802 (2012).
[15] K. Abe et al., [arXiv:1109.3262] [Search INSPIRE].
[16] Z. Maki, M. Nakagawa, and S. Sakata, Prog. Theor. Phys. **28**, 870 (1962).
[17] B. Pontecorvo, Sov. Phys. JETP **26**, 984 (1968).
[18] K. A. Olive et al., Chin. Phys. C **38**, 090001 (2014).
[19] J. Schechter and J. W. F. Valle, Phys. Rev. D **22**, 2227 (1980).
[20] S. M. Bilenky, J. Hosek, and S. T. Petcov, Phys. Lett. B **94**, 495 (1980).
[21] M. Doi, T. Kotani, H. Nishiura, K. Okuda, and E. Takasugi, Phys. Lett. B **102**, 323 (1981).
[22] V. D. Barger, K. Whisnant, and R. J. N. Phillips, Phys. Rev. Lett. **45**, 2084 (1980).
[23] S. Pakvasa, AIP Conf. Proc. **68**, 1164 (1980).
[24] C. Jarlskog, Phys. Rev. Lett. **55**, 1039 (1985).
[25] F. Capozzi et al., Phys. Rev. D **89**, 093018 (2014).
[26] S. Pascoli, S. T. Petcov, and A. Riotto, Phys. Rev. D **75**, 083511 (2007).
[27] S. Pascoli, S. T. Petcov, and A. Riotto, Nucl. Phys. B **774**, 1 (2007).
[28] Q. R. Ahmad et al., Phys. Rev. Lett. **89**, 011301 (2002).
[29] K. Abe et al., Phys. Rev. D **83**, 052010 (2011).
[30] K. Eguchi et al., Phys. Rev. Lett. **90**, 021802 (2003).
[31] T. Araki et al., Phys. Rev. Lett. **94**, 081801 (2005).
[32] S. Abe et al., Phys. Rev. Lett. **100**, 221803 (2008).
[33] Y. Ashie et al., Phys. Rev. D **71**, 112005 (2005).
[34] Y. Ashie et al., Phys. Rev. Lett. **93**, 101801 (2004).
[35] M. H. Ahn et al., Phys. Rev. D **74**, 072003 (2006).
[36] P. Adamson et al., Phys. Rev. Lett. **106**, 181801 (2011).
[37] K. Abe et al., Phys. Rev. D **85**, 031103 (2012).
[38] K. Abe et al., Phys. Rev. Lett. **112**, 181801 (2014).
[39] P. Adamson et al., Phys. Rev. Lett. **107**, 181802 (2011).
[40] K. Abe et al., Phys. Rev. D **88**, 032002 (2013).
[41] Y. Abe et al., Phys. Rev. Lett. **108**, 131801 (2012).
[42] F. P. An et al., Phys. Rev. Lett. **108**, 171803 (2012).
[43] J. Arafune, M. Koike, and J. Sato, Phys. Rev. D **56**, 3093 (1997).
[44] P. Adamson et al., Phys. Rev. Lett. **112**, 191801 (2014).
[45] A. Himmel, AIP Conf. Proc. **1604**, 345 (2014).
[46] S. F. King and C. Luhn, Rept. Prog. Phys. **76**, 056201 (2013).
[47] C. H. Albright, A. Dueck, and W. Rodejohann, Eur. Phys. J. C **70**, 1099 (2010).
[48] G. Altarelli and F. Feruglio, Rev. Mod. Phys. **82**, 2701 (2010).
[49] H. Ishimori et al., Prog. Theor. Phys. Suppl. **183**, 1 (2010).
[50] C. H. Albright and M. C. Chen, Phys. Rev. D **74**, 113006 (2006).
[51] R. N. Mohapatra and A. Y. Smirnov, Ann. Rev. Nucl. Part. Sci. **56**, 569 (2006).
[52] Y. Yamazaki et al., Accelerator technical design report for J-PARC (2003), KEK-REPORT-2002-13, JAERI-TECH-2003-044, J-PARC-03-01.
[53] T. Koseki, J-PARC Accelerator —status, capacity and future plan— (July 2014), Talk presented at the 2nd international symposium on science at J-PARC (J-PARC 2014), Tsukuba, Japan.
[54] S. Igarashi, H. Harada, H. Hotchi, T. Koseki, and Y. Sato, Accelerator Concepts for the Beam Power of Multi MW with J-PARC MR (July 2014), Talk presented at the 2nd international symposium on science at J-PARC (J-PARC 2014), Tsukuba, Japan.
[55] K. Abe et al., Nucl. Instrum. Meth. A **659**, 106 (2011).
[56] T. Sekiguchi, Prog. Theor. Exp. Phys. **2012**, 02B005 (2012).

[57] D. Beavis et al., Long Baseline Neutrino Oscillation Experiment at the AGS(Proposal E889), Physics Design Report, BNL-52459 (1995).
[58] T. Ishida, [arXiv:1411.5540] [Search INSPIRE].
[59] M. Otani et al., Nucl. Instrum. Meth. A **623**, 368 (2010).
[60] S. Assylbekov et al., Nucl. Instrum. Meth. A **686**, 48 (2012).
[61] N. Abgrall et al., Nucl. Instrum. Meth. A **637**, 25 (2011).
[62] P. A. Amaudruz et al., Nucl. Instrum. Meth. A **696**, 1 (2012).
[63] D. Allan et al., J. Instrum. **8**, P10019 (2013).
[64] S. Aoki et al., Nucl. Instrum. Meth. A **698**, 135 (2013).
[65] T2K Collaboration, *Physics potential and sensitivities of T2K* (2013). (Available at: http://www.t2k.org/docs/pub/015, date last accessed April 20, 2015) T2K Report to 17th J-PARC PAC, September 2013.
[66] M. Yeh et al., Nucl. Instrum. Meth. A **660**, 51 (2011).
[67] K. Abe et al., *A letter of intent to extend T2K with a detector 2 km away from the JPARC neutrino source* (2007). (Available at: http://j-parc.jp/researcher/Hadron/en/pac_0707/pdf/2km-loi-final-070628.pdf, date last accessed April 20, 2015).
[68] A. A. Aguilar-Arevalo et al., Nucl. Instrum. Meth. A **599**, 28 (2009).
[69] J. F. Beacom and M. R. Vagins, Phys. Rev. Lett. **93**, 171101 (2004).
[70] *GitHub repository for WCSim*. (Available at: https://github.com/WCSim/WCSim, date last accessed April 20, 2015).
[71] S. Agostinelli et al., Nucl. Instrum. Meth. A **506**, 250 (2003).
[72] J. Allison et al., IEEE Trans. Nucl. Sci. **53**, 270 (2006).
[73] R. B. Patterson et al., Nucl. Instrum. Meth. A **608**, 206 (2009).
[74] K. Hagiwara, N. Okamura, and K. Senda, J. High Energy Phys. **1109**, 082 (2011).
[75] C. Adams et al., [arXiv:1307.7335] [Search INSPIRE].
[76] S. K. Agarwalla et al., [arXiv:1412.0593] [Search INSPIRE].
[77] K. Abe et al., Prog. Theor. Exp. Phys. **2015**, 043C01 (2015).
[78] K. Abe et al., Phys. Rev. D **87**, 012001 (2013).
[79] N. Abgrall et al., Phys. Rev. C **84**, 034604 (2011).
[80] N. Abgrall et al., Phys. Rev. C **85**, 035210 (2012).
[81] N. Abgrall et al., Nucl. Instrum. Meth. A **701**, 99 (2013).
[82] Y. Hayato, Nucl. Phys. Proc. Suppl. **112**, 171 (2002).
[83] G. Mitsuka, AIP Conf. Proc. **967**, 208 (2007).
[84] G. Mitsuka, AIP Conf. Proc. **981**, 262 (2008).
[85] R. Brun, F. Carminati, and S. Giani: GEANT Detector Description and Simulation Tool, CERN-W5013 (1994).
[86] M. Day and K. S. McFarland, Phys. Rev. D **86**, 053003 (2012).
[87] G. L. Fogli and E. Lisi, Phys. Rev. D **54**, 3667 (1996).
[88] H. Minakata, H. Sugiyama, O. Yasuda, K. Inoue, and F. Suekane, Phys. Rev. D **68**, 033017 (2003).
[89] K. Hiraide et al., Phys. Rev. D **73**, 093008 (2006).